

EVALUATION OF EXPOSURE DOSES RESULTING FROM SCINTILLATION AND
IONIZATION DETECTOR MEASUREMENTS OF COMPLEX GAMMA-RAY SPECTRA

by

45

WILLIAM THOMAS URBAN

B. S., Kansas State University, 1964

A MASTER'S THESIS

submitted in partial fulfillment of the
requirements for the degree

MASTER OF SCIENCE

Department of Nuclear Engineering

KANSAS STATE UNIVERSITY

Manhattan, Kansas

1969

Approved by



Major Professor

TABLE OF CONTENTS

	Page
1.0 INTRODUCTION.....	1
2.0 THEORETICAL DEVELOPMENT.....	4
2.1 Unfolding Technique.....	4
2.2 Design of an Appropriate Experiment.....	6
2.3 Calibration of the Dosimeter.....	9
3.0 EXPERIMENTAL APPARATUS.....	19
4.0 EXPERIMENTAL PROCEDURE.....	25
5.0 CALIBRATION OF THE DOSIMETER LOCATED WITHIN THE COLLIMATOR....	31
6.0 DISCUSSION OF RESULTS.....	41
7.0 CONCLUSIONS.....	55
8.0 SUGGESTIONS FOR FURTHER STUDY.....	56
9.0 ACKNOWLEDGEMENT.....	58
10.0 LITERATURE CITED.....	59
11.0 APPENDICES.....	62
APPENDIX A: SPECTROMETER QUALITY CONTROL.....	63
APPENDIX B: CALIBRATION OF THE COBALT-60 SIMULATED PLANE ISOTROPIC SOURCE.....	68
APPENDIX C: CALIBRATION OF THE DOSIMETER USING A POINT SOURCE.....	73
APPENDIX D: REGRESSION ANALYSIS.....	82
APPENDIX E: UNCOLLIDED GAMMA-RAY FLUX IN THE COLLIMATOR RESULTING FROM VARIOUS PLANE SOURCE ANGULAR DISTRIBUTIONS.....	87

LIST OF TABLES

I.	Experimental configurations and corresponding energies of once scattered gamma rays.....	36
II.	Values of (R_s/R_{E_1}) and $(\mathcal{D}R_m^S(\mu_a)/\mathcal{D}R_m^{E_1}(\mu_a))$ for each experimental configuration, based on energies of once scattered gamma rays.....	37
III.	Data used to determine the equation of the calibration line for the P_1 configuration.....	38
IV.	Comparison of spectral and dosimeter exposure doses.....	48
B-1.	Experimental dosimeter responses and their corresponding average doses used in the calibration of the simulated plane source.....	70
C-1.	Data used in the calibration of the dosimeter using a point source....	78
E-1.	Normalized fluxes as a function of position in the collimator and plane source angular distribution.....	93

LIST OF FIGURES

1.	Dosimeter response versus exposure dose for exposure of a dosimeter to a monoenergetic plane source (slope = k_{E_1}) and a polyenergetic plane source (slope = k_s).....	17
2.	Machine drawing of the collimator system.....	20
3.	Line source consisting of eighteen cobalt-60 sources.....	23
4.	Plane simulator.....	24
5.	Experimental configuration used in the unfolding confirmation.....	26
6.	Experimental configuration for the collimator-dosimeter calibration.....	28
7.	Schematic of experiments and calculations performed in the confirmation of the unfolding codes.....	30
8.	Original and unfolded spectra for the P_1 configuration.....	42
9.	Original and unfolded spectra for the P_2 configuration.....	43
10.	Original and unfolded spectra for the P_3 configuration.....	44
11.	Experimental configuration for the plane source calibration.....	69
12.	Experimental configuration for the dosimeter calibration using a point source.....	74
13.	Collimator-source geometry used in the derivation of the uncollided flux as a function of position within the collimator.....	88

NOMENCLATURE

B_1	buildup factor for air scattering
B_2	buildup factor for ground scattering
\bar{C}	column vector for the experimentally observed gamma-ray spectrum
$d^2\Omega$	differential solid angle (see Eq. (E-2))
D_p	strength of the simulated plane source of cobalt-60 (mr/28 min.)
D_z	exposure dose in mr for detector at a distance z from the plane source
D	exposure dose obtained from the unfolded pulse height distribution
$D_{Th}^{E_1}(\text{mr})$	theoretical exposure dose due to a plane source emitting gamma rays of energy E_1
$D_{Th}^S(\text{mr})$	theoretical exposure doses due to a plane source emitting gamma rays with a spectrum of energies
$\mathcal{D}_{Th}^{E_1}(\text{mr})$	theoretical exposure dose due to a point source emitting gamma rays of energy E_1
$\mathcal{D}_{Th}^S(\text{mr})$	theoretical exposure dose due to a point source emitting gamma rays with a spectrum of energies
$\theta_{DR_m}^{E_1}(\mu\text{a})$	experimental dosimeter response due to a plane source emitting gamma rays of energy E_1
$\theta_{DR_m}^S(\mu\text{a})$	experimental dosimeter response due to a plane source emitting gamma rays with a spectrum of energies
$\mathcal{D}R_m^{E_1}(\mu\text{a})$	experimental dosimeter response due to a point source emitting gamma rays of energy E_1
$\mathcal{D}R_m^S(\mu\text{a})$	experimental dosimeter response due to a point source emitting gamma rays with a spectrum of energies
E_1	average energy of gamma rays emitted by cobalt-60, 1.25 MeV
E_{ss}	once scattered gamma-ray energy (MeV)
E_i	average energy of the i^{th} energy bin
$E[w]$	expected value of the quantity w

G	conversion factor (mr-gm/MeV)
K	conversion factor ((mr/hr)/(mc/cm))
k_E	proportionality constant relating $DR_m^E (\mu a)$ to $D_{Th}^E (mr)$
k_s	proportionality constant relating $DR_m^S (\mu a)$ to $D_{Th}^S (mr)$
k_{E_1}	proportionality constant relating $\mathcal{D}R_m^E (\mu a)$ to $\mathcal{D}_{Th}^E (mr)$
k_s	proportionality constant relating $\mathcal{D}R_m^S (\mu a)$ to $\mathcal{D}_{Th}^S (mr)$
ℓ	number of degrees of freedom
m	number of experimental observations of which \bar{y}' is the mean
$m_0 c^2$	rest energy of an electron (MeV)
\bar{N}	column vector representing the unfolded pulse height distribution
N_i	number of gamma rays per cm^2 in the i^{th} energy bin
P_1, P_2, P_3	experimental configurations considered
P	atmospheric pressure (inches of mercury)
Q	sum of the residuals squared in regression analysis
R_0	radius of collimator
\bar{R}	response matrix for the collimator spectrometer system
R_{E_1}	collimator correction factor for gamma rays of energy E_1 (see Eq. (5))
R_s	collimator correction factor for gamma rays with a spectrum of energies
r	distance between source and detector
S	strength of calibrated point source on the date of its use
$S(\Omega)$	source angular distribution
S_i	strength of calibrated point source on the date of its calibration
$(s)^2$	estimated variance
$(s')^2$	estimated variance using the Berkson model for controlled experiments

T	temperature in degrees Fahrenheit
t	fractional point of the Student's distribution
$t_{1/2}$	half-life of cobalt-60 in years
$V[w]$	variance of w
w	defined by Eq. (D-14)
(x_i, y_i)	data point used in the regression analysis (x_i represents exposure dose in mr and y_i represents dosimeter response in μa)
Y_i	function x_i representing the estimated regression line
\bar{y}'	mean value of m observations of the dosimeter response
z	perpendicular distance between plane source and a point in the collimator

Greek Symbols

α	temperature and pressure correction factor applied to the experimental dosimeter responses
$\alpha_{\theta}^{E_1}$	dosimeter angular correction factor for gamma rays of energy E_1
α_{θ}^s	dosimeter angular correction factor for gamma rays with a spectrum of energies
β	true slope which is estimated by b in the regression analysis
γ	expected value corresponding to the observed value y
η	value of \bar{y}' corresponding to the value of x if the true regression line were used
θ_0	polar angle defining the angle of incidence for a gamma ray striking a slab
θ	polar angle defining the angle of emergence for gamma rays which have been scattered from a slab
θ_1	angle defining the collimator aperture
θ_s	gamma-ray scattering angle
$(\mu\text{a}/\rho)$	gamma-ray energy absorption mass attenuation coefficient (cm^2/gm)

ν, ξ, μ	dimensionless parameters used in describing the collimator-source geometry of Appendix E
σ^2	true variance
ϕ	azimuthal angle used in defining the gamma-ray scattering angle for gamma rays scattered from a slab
ϕ_E	energy flux per roentgen
$\phi^i(\nu, \xi)$	uncollided gamma-ray flux as a function of the dimensionless collimator parameters ν and ξ , $i = I, II, III$ (see pages 90 and 91)

1.0 INTRODUCTION

Since the development of the scintillation detector and the pulse-height analyzer a significant amount of work has been done in the area of gamma-ray spectroscopy. However, the pulse-height spectrum obtained through the use of such a system is not a proportional representation of the energy spectrum of gamma rays striking the scintillation detector. This is the result of distortions in both the scintillation detector crystal and the associated electronic equipment, together comprising the gamma-ray spectrometer system.

With the realization that the experimentally observed spectrum is not an accurate representation of the true energy spectrum, a number of mathematical techniques (1-9) have been proposed to enable the determination of the true gamma-ray energy spectrum from the experimental spectrum. These techniques are referred to as unfolding and since they usually require the use of high speed computers they are commonly known as unfolding codes.

Although each of these unfolding techniques has its merit there are variations in the mathematical approaches used in arriving at the solutions as well as the physical models on which they are based. Hence the application of a particular unfolding technique may vary with experimenters because of dissimilarities in scintillation spectrometer systems. Therefore, even though a general unfolding technique is used, each experimenter must develop an unfolding code which will accurately describe the distortions introduced into the experimentally observed spectrum by the scintillation spectrometer system and also take into account the experimental environment in which the measurements were made.

Many papers (1,2,4,6,7,8) have been published listing the results of the applications of unfolding codes for a variety of detection systems and experimental environments. However, there has not been available a generally accepted method for determining how well the unfolded spectrum represents the true energy spectrum of radiation incident upon the detector. Unfolding codes are often confirmed by applying them to a "standard complex spectrum." A spectrum of this type is generated by combining spectra resulting from standard monoenergetic sources. Then the gamma-ray energies and their intensities which are obtained by unfolding the "standard complex spectrum" can be compared to the energies and intensities of the standard monoenergetic sources. The problem with using such a method is that the unfolding codes are based on spectrometer system responses to standard monoenergetic sources such as used to generate the "standard complex spectrum." Therefore this procedure does not really test the validity of the unfolding code for gamma rays whose energies are different from those of the standard monoenergetic sources. In practice such spectra are often encountered. In addition, the energies of the gamma rays incident upon the detector are often nearly equal and therefore their individual contributions to the complex spectrum can not readily be determined. In this case one does not know either the number or the energies of the gamma rays which contribute to the complex spectrum and therefore it is difficult to theoretically predict the shape and intensity of the true energy distribution.

The purpose of this work has been to determine experimentally the validity of using an unfolding code, developed for a collimator-spectrometer system, as a tool in the computation of exposure doses resulting from experimentally measured complex spectra. This determination is based on a

comparison of exposure doses computed on the basis of measured complex gamma-ray energy spectra with exposure doses measured with an air equivalent ionization chamber. Although this report is concerned with the accuracy of exposure doses calculated using an unfolding code, a detailed analysis of the unfolding code in question is not intended.

2.0 THEORETICAL DEVELOPMENT

2.1 Unfolding Technique

In the design of an experiment to determine the accuracy and thereby obtain a measure of the validity of an unfolding technique, the first requirement is a basic understanding of the technique in question. Hence it is imperative to know under what experimental conditions the technique is applicable, the general principles involved and the form in which results are obtained as well as what they represent.

The unfolding technique under investigation in this report was developed by J. A. Baran (10) as a result of a research project sponsored by the Department of Defense Office of Civil Defense under Contract OCD-OS-63-74. The primary purpose of this technique was to provide a method for determining the true gamma-ray energy spectrum from an experimentally measured pulse-height distribution. A knowledge of the true gamma-ray energy spectrum was necessary for the computation of differential exposure doses resulting from the scattering of gamma rays from small areas on a concrete slab. Scattering of gamma rays from concrete results in an emergent flux of gamma rays with a distribution of energies, i.e., a plane source of polyenergetic gamma rays.

The experimental apparatus for which this technique was developed consisted of a scintillation detector located within a collimator and a pulse-height analyzer. Hereinafter this group of instruments will be referred to as the collimator-spectrometer system. Since the source to which the detector was exposed consisted of scattered gamma rays, the unfolding technique was formulated to analyze complex gamma-ray spectra over a wide range of gamma-ray energies.

A detailed development of this unfolding technique is beyond the scope of this report; however, a complete analysis, including computer codes, is available in reference 10. For the purposes of this report, the problem of unfolding can be simply stated through the use of the matrix equation

$$\bar{C} = \bar{R} \bar{N} \quad (1)$$

where \bar{C} is the experimentally observed spectrum,

\bar{R} is a response matrix and

\bar{N} is the desired unfolded pulse-height distribution.

In the above equation, \bar{C} and \bar{N} are column vectors and \bar{R} is a square matrix. The response matrix, which relates the experimental spectrum to the unfolded pulse-height distribution, corrects the experimental spectrum for the distortions introduced by the collimator-spectrometer system, i.e., the scintillation detector, the collimator and the associated electronics used in making the experimental measurements. This matrix was obtained by considering the response of the system to a number of calibrated monoenergetic gamma-ray sources over the energy range of interest.

Solving Eq. (1) for the unfolded pulse-height distribution results in

$$\bar{N} = \bar{R}^{-1} \bar{C} . \quad (2)$$

The unfolded pulse-height distribution obtained from this equation is thus a measure of the energy distribution of the gamma-ray flux at the center of the crystal. It should be noted that this pulse-height distribution has been corrected for the effects of the collimator, i.e., the distortion in the collimator, as well as the response of the spectrometer system.

2.2 Design of an Appropriate Experiment

With the preceding discussion concerning the conditions under which the unfolding technique is applicable and an understanding of what the results represent, an appropriate experiment can be designed to determine the accuracy of this technique. However, at this point, it is advantageous to examine this problem in general before considering the design of an experiment for this particular technique.

In general the problem of determining the accuracy of a particular technique which is to be used in the calculation of a specific experimentally observable physical phenomenon often results in a pseudo calibration of the technique in question. When confronted with such a problem, a logical solution is to design an experiment such that the quantity to be measured is either known precisely or can be obtained directly using another method whose accuracy has previously been established. Assuming that such an experiment can be designed and carried out, then a comparison of the value which was determined experimentally, using the technique under investigation, to the known or accepted value will be a measure of the accuracy of the procedure in question.

However, it is often found that in the use of such an experiment to determine the accuracy of a specific technique, the value of the quantity to be measured experimentally neither is known precisely nor can it be calculated directly from theoretical considerations alone. When this is the case a generally accepted course of action is to determine the standard or accepted value by experimentally measuring the same quantity using a completely independent method, whose accuracy can be well established.

In order to determine the accuracy of the unfolding technique, the experiment to be designed must be such that the resulting confidence on this technique will be valid under the conditions for which it is to be used. Thus a complex gamma-ray spectrum must be investigated if this technique is to be properly evaluated. Any theoretical evaluation of the unfolding technique would therefore require a knowledge of the gamma-ray energy distribution under investigation. Since calibrated plane sources emitting gamma rays over a wide energy range are nonexistent, such plane sources must necessarily be simulated. The simulation of such a source would then make it necessary to calculate the energy distribution of the gamma-ray flux under investigation and such a calculation would be quite involved, and then only an approximation. Thus it is advantageous to determine the standard value experimentally. These values could then be compared to the results of the collimator-spectrometer measurements in order to determine the accuracy of the unfolding technique.

Hence an experiment designed to fulfill the objectives of this report must meet the following requirements:

1. a plane source emitting gamma rays over a spectrum of energies must be used in the experimental measurements,
2. measurements must be made using several different plane sources,
3. a detector must be selected which can be used in the same experimental configuration as the scintillation detector, and
4. the quantities measured using the detector of 3. must be comparable to those obtained from the unfolding technique.

Requirement 1. is necessary in order that a nontrivial determination of the accuracy is made and the second is primarily for the purpose of revealing any

systematic errors. The detector selected to be used in the independent measurements must be of reputable accuracy, must have physical dimensions compatible with the collimator and must result in a quantity which can be directly compared to the results obtained using the unfolding technique.

An air equivalent ionization chamber (dosimeter) which can be accurately calibrated, obtained in a variety of physical sizes, and used to measure a quantity directly proportional to the exposure dose, meets all of the previously mentioned requirements for the detector to be used in the measurements. In addition, the response of the dosimeter is linear with respect to the dose received. Although the quantity measured by the dosimeter is proportional to exposure dose and that obtained from the spectral measurements is a pulse-height distribution, both measurements may readily be converted to exposure dose. In fact, the prime objective of this work was to determine how accurately exposure doses could be determined using the unfolding technique to analyze the spectral data obtained using the collimator-spectrometer system.

Thus the experiment used to determine the accuracy of the unfolding technique will involve the comparison of exposure doses obtained from dosimeter and collimator-spectrometer measurements. Both methods of measuring the exposure dose must be carried out using the same experimental geometry and plane source. The dosimeter measurements must necessarily be carried out with care in order that the exposure dose obtained can be accepted with confidence as a correct measure of the exposure dose.

2.3 Calibration of the Dosimeter

Since the measure of the accuracy of the unfolding technique can be only as good as the dosimeter measurements, the dosimeter must be accurately calibrated. As the dosimeter is an indirect reading instrument, calibration of the dosimeter is necessary if an exposure dose is to be obtained.

In the preceding section it was stated that the dosimeter and collimator-spectrometer measurements must be made using the same plane sources and experimental configurations. This implies that the dosimeter must be calibrated while located within the collimator and exposed to a plane source of gamma radiation.

Thus the calibration curve must relate the dosimeter response, which is in microamperes (μa), to an exposure dose in milliroentgens (mr) based on an exposure to a plane source emitting gamma rays with an energy distribution identical to that which will be encountered in the experiment to determine the accuracy of the unfolding technique. In addition the calibration must take into account the effects of the collimator so that the dosimeter results can be directly compared to the exposure doses obtained from the collimator-spectrometer measurements.

Such a calibration would normally be performed by exposing the dosimeter to a calibrated source of radiation and then plotting the measured dosimeter response versus the theoretically computed exposure dose which would be expected at the center of the dosimeter. However, since calibrated plane polyenergetic sources are not readily available, as was previously mentioned, a method of calibrating the dosimeter using a calibrated monoenergetic plane source is necessary. This calibration must incorporate within it corrections for the effects of the collimator and the energy dependence of the dosimeter.

First assume that it is possible to obtain a calibration of the dosimeter in air and exposed to a calibrated monoenergetic point source which emits gamma rays with energy E_1 . Thus a relationship of the form

$$\mathcal{D}_m^{R E_1}(\mu a) = k_{E_1} \mathcal{D}_{Th}^{E_1}(\text{mr}) \quad (3)$$

can be obtained, where $\mathcal{D}_m^{R E_1}(\mu a)$ is the experimentally measured dosimeter response, $\mathcal{D}_{Th}^{E_1}(\text{mr})$ is the theoretical exposure dose which would be expected at the center of the dosimeter and k_{E_1} is the proportionality constant relating the preceding two quantities.

Now let $\alpha_\theta^{E_1}$ be an angular correction factor defined as the ratio of the dosimeter response for radiation of energy E_1 incident normal to the axis of the dosimeter to its response for radiation of energy E_1 incident at some angle θ to the axis of the dosimeter. Further assume that the dosimeter calibration resulting in Eq. (3) was conducted such that $\alpha_\theta^{E_1}$ is unity.

The dosimeter must next be placed in the collimator and exposed to a calibrated plane source of radiation. Ideally this plane source would emit gamma rays with an energy distribution identical to that which would be investigated in the collimator-spectrometer measurements; however, since calibrating the dosimeter in the collimator requires a theoretical calculation of the exposure dose, this is not feasible. Also such a calibrated plane source is not available. Therefore a calibrated monoenergetic plane source must be used to calibrate the dosimeter in this geometric configuration and appropriate corrections made to account for the fact that the calibration curve is to be used in the measurement of radiation emitted from a polyenergetic plane source rather than a monoenergetic plane source.

Consider the following terms which will be used in describing the calibration of the dosimeter located in the collimator and exposed to a monoenergetic plane source:

${}_{\theta}DR_m^{E_1}(\mu a)$ = experimentally measured dosimeter response to a monoenergetic plane source emitting gamma rays of energy E_1 which are incident on the dosimeter at an angle θ to the axis of the dosimeter,

$D_{Th}^{E_1}(\text{mr})$ = theoretical exposure dose resulting from exposure to the plane source emitting gamma rays of energy E_1 .

The quantity ${}_{\theta}DR_m^{E_1}(\mu a)$ is the response of the dosimeter due to direct radiation plus that radiation which reaches the detector as a result of interactions with the collimator. However, $D_{Th}^{E_1}(\text{mr})$ represents the exposure dose which would be expected as a result of direct radiation alone. Direct radiation is considered to be those gamma rays which are emitted from the source in such a direction that they can reach the detector without the need of an intermediate scatter. Therefore, when discussing the plane source measurements using the collimator, direct radiation refers to that radiation emanating from the disk on the source plane subtended by the solid angle of the collimator. The theoretical dosimeter response ${}_{\theta}D_{Th}^{E_1}(\mu a)$ resulting from exposure of the dosimeter, located within the collimator, to a monoenergetic plane source emitting gamma rays of energy E_1 which are incident on the dosimeter at an angle θ to the dosimeter axis, can be computed using Eq. (3) to obtain

$${}_{\theta}D_{Th}^{E_1}(\mu a) = \frac{1}{\alpha_{\theta}^{E_1}} k_{E_1} D_{Th}^{E_1}(\text{mr}) . \quad (4)$$

Now define the collimator correction factor for the energy E_1 as

$$R_{E_1} = \frac{\theta_{DR_m}^{E_1}(\mu a)}{\theta_{D_{Th}}^{E_1}(\mu a)} . \quad (5)$$

R_{E_1} actually represents the ratio of the dosimeter response for direct radiation plus that radiation reaching the detector as a result of collimator interactions to the response resulting from direct radiation alone. Combining Eq. (4) and Eq. (5) yields

$$\theta_{DR_m}^{E_1}(\mu a) = R_{E_1} \theta_{D_{Th}}^{E_1}(\mu a) = R_{E_1} \frac{k_{E_1} D_{Th}^{E_1}(\text{mr})}{\alpha_{\theta}^{E_1}} . \quad (6)$$

Next consider a point source which emits gamma rays with an energy distribution identical to that which is to be investigated in the measurements for determining the accuracy of the unfolding technique. Assume that this point source, when used in the same geometry as the monoenergetic point source used in determining Eq. (3), results in an exposure dose $\mathcal{D}_{Th}^S(\text{mr})$ such that

$$\mathcal{D}_{Th}^{E_1}(\text{mr}) = \mathcal{D}_{Th}^S(\text{mr}) . \quad (7)$$

Calibrating the dosimeter under the same conditions as used in obtaining Eq. (3) results in the relation

$$\mathcal{D}R_m^S(\mu a) = k_s \mathcal{D}_{Th}^S(\text{mr}) \quad (8)$$

where $\mathcal{D}R_m^S(\mu a)$ = dosimeter response in microamperes resulting from gamma rays, with the energy distribution previously described, incident normal to the axis of the dosimeter,

k_s = the proportionality constant relating the dosimeter response to the exposure dose for this point source.

Now assume that a calibrated plane source is available which emits gamma rays with an energy distribution identical to that simulated for the dosimeter and collimator-spectrometer measurements. Further assume that this plane source is such that

$$D_{Th}^{E1}(mr) = D_{Th}^S(mr) \quad (9)$$

where $D_{Th}^{E1}(mr)$ and $D_{Th}^S(mr)$ are the theoretical exposure doses which would be expected respectively for the dosimeter located within the collimator and exposed to the monoenergetic and polyenergetic plane sources.

Define ${}_{\theta}DR_m^S(\mu a)$ as the response of the dosimeter located within the collimator resulting from an exposure to the polyenergetic plane source where the radiation is incident at an angle θ to the axis of the dosimeter. Then in a manner similar to that used for the monoenergetic plane source the relation between the dosimeter response and the theoretical exposure dose, ${}_{\theta}D_{Th}^S(\mu a)$, can be represented by

$${}_{\theta}DR_m^S(\mu a) = R_s {}_{\theta}D_{Th}^S(\mu a) , \quad (10)$$

or

$${}_{\theta}DR_m^S(\mu a) = R_s \frac{k_s D_{Th}^S(mr)}{\alpha_{\theta}^S} \quad (11)$$

where R_s = the collimator correction factor for the gamma-ray energy distribution now being considered (R_s is analogous to R_{E1} as defined by Eq. (5)),

α_{θ}^S = the angular correction factor of the dosimeter for gamma radiation with the energy distribution now being considered.

Using Eq. (9), then Eq. (11) can be written as

$${}_{\theta}DR_m^S(\mu a) = \frac{R_s k_s D_{Th}^{E1}(\text{mr})}{\alpha_{\theta}^S}, \quad (12)$$

and using Eq. (6) a substitution for $D_{Th}^{E1}(\text{mr})$ can be made to obtain

$${}_{\theta}DR_m^S(\mu a) = \frac{R_s k_s}{\alpha_{\theta}^S} \left[\frac{\alpha_{\theta}^{E1} {}_{\theta}DR_m^{E1}(\mu a)}{k_{E1} R_{E1}} \right]. \quad (13)$$

Combining Eqs. (12) and (13) yields

$${}_{\theta}DR_m^S(\mu a) = \left[\frac{R_s}{R_{E1}} \right] \left[\frac{\alpha_{\theta}^{E1}}{\alpha_{\theta}^S} \right] \left[\frac{k_s}{k_{E1}} \right] {}_{\theta}DR_m^{E1}(\mu a) = \frac{R_s k_s}{\alpha_{\theta}^S} D_{Th}^{E1}(\text{mr}). \quad (14)$$

Hence, using Eq. (14), a calibration curve could be obtained which would be applicable for the gamma-ray energy distribution which is to be measured. This can be done by plotting the middle group of terms, i.e., the group containing ${}_{\theta}DR_m^{E1}(\mu a)$, versus the theoretical dose, $D_{Th}^{E1}(\text{mr})$, and then using a regression line to fit these points. The slope of this line would then be equivalent to $(R_s k_s)/\alpha_{\theta}^S$.

However, if a calibration curve is to be determined using Eq. (14), evaluation of the ratios (R_s/R_{E1}) , $(\alpha_{\theta}^{E1}/\alpha_{\theta}^S)$ and (k_s/k_{E1}) is necessary. First consider $(\alpha_{\theta}^{E1}/\alpha_{\theta}^S)$. With the definition of the two terms in this ratio, this ratio can be expressed as

$$\frac{\alpha_{\theta}^{E_1}}{\alpha_{\theta}^S} = \frac{\left[\frac{\mathcal{D}R_m^{E_1}(\mu a)}{\mathcal{D}R_m^{E_1}(\mu a)} \right]}{\left[\frac{\mathcal{D}R_m^S(\mu a)}{\mathcal{D}R_m^S(\mu a)} \right]} . \quad (15)$$

Using the relations for k_s and k_{E_1} given by Eqs. (3) and (8) yields

$$\frac{k_s}{k_{E_1}} = \frac{\left[\frac{\mathcal{D}R_m^S(\mu a)}{\mathcal{D}_{Th}^S(\text{mr})} \right]}{\left[\frac{\mathcal{D}R_m^{E_1}(\mu a)}{\mathcal{D}_{Th}^{E_1}(\text{mr})} \right]} . \quad (16)$$

Since $\mathcal{D}_{Th}^S(\text{mr}) = \mathcal{D}_{Th}^{E_1}(\text{mr})$, Eq. (16) can be reduced to

$$\frac{k_s}{k_{E_1}} = \frac{\mathcal{D}R_m^S(\mu a)}{\mathcal{D}R_m^{E_1}(\mu a)} . \quad (17)$$

Thus the product of Eqs. (15) and (17) results in

$$\frac{\alpha_{\theta}^{E_1} k_s}{\alpha_{\theta}^S k_{E_1}} = \frac{\mathcal{D}R_m^S(\mu a)}{\mathcal{D}R_m^{E_1}(\mu a)} . \quad (18)$$

Substitution of Eq. (18) into Eq. (14) yields

$$\mathcal{D}_{\theta}^{DR_m^S}(\mu a) = \frac{R_s}{R_{E_1}} \left[\frac{\mathcal{D}R_m^S(\mu a)}{\mathcal{D}R_m^{E_1}(\mu a)} \right] \mathcal{D}_{\theta}^{DR_m^{E_1}}(\mu a) = \frac{R_s k_s}{\alpha_{\theta}^S} \mathcal{D}_{Th}^{E_1}(\text{mr}) . \quad (19)$$

In order to evaluate the ratios (R_s/R_{E_1}) and $(\mathcal{D}_{\theta}^{DR_m^S}(\mu a)/\mathcal{D}_{\theta}^{DR_m^{E_1}}(\mu a))$, it is necessary to know the energy distribution of gamma rays emitted from the polyenergetic plane source. It was noted previously that it would be

possible, although quite tedious, to obtain this energy distribution from theoretical considerations. However, since the dosimeter measures a quantity which is proportional to exposure dose integrated over time and energy, only the average energy of the energy distribution under consideration is necessary. This average energy can be approximated by the single scattered gamma-ray energy which can be computed using the scattering angle defined by the experimental configuration under investigation. The validity of this approximation will be discussed in Section 5.0. Then if both the collimator correction factor and the dosimeter response can be expressed, either experimentally or theoretically, as a function of gamma-ray energy, the ratios (R_s/R_{E_1}) and $(\theta DR_m^S(\mu a)/\theta DR_m^{E_1}(\mu a))$ can be evaluated using the single scattered energies.

To obtain a better interpretation of the physical significance of Eq. (19), consider the following graphical approach. First write Eq. (6) in the form

$$\theta DR_m^{E_1}(\mu a) = k_{E_1} D_{Th}^{E_1}(\text{mr}) \quad (20)$$

where $k_{E_1} = R_{E_1} k_{E_1} / \alpha_{\theta}^{E_1}$. In a similar manner, Eq. (12) can be written in the form

$$\theta DR_m^S(\mu a) = k_s D_{Th}^{E_1}(\text{mr}) \quad (21)$$

where $k_s = R_s k_s / \alpha_{\theta}^S$. Solving Eqs. (20) and (21) for $D_{Th}^{E_1}(\text{mr})$ yields the relation

$$\frac{\theta DR_m^{E_1}(\mu a)}{k_{E_1}} = \frac{\theta DR_m^S(\mu a)}{k_s} = D_{Th}^{E_1}(\text{mr}) \quad , \quad (22)$$

or

$$\theta DR_m^S(\mu a) = \frac{k_s}{k_{E_1}} \theta DR_m^{E_1}(\mu a) \quad . \quad (23)$$

Comparing this result with

$$\theta^{DR_m^S}(\mu a) = \frac{R_s}{R_{E_1}} \left[\frac{\theta^{DR_m^S}(\mu a)}{\theta^{DR_m^{E_1}}(\mu a)} \right] \theta^{DR_m^{E_1}}(\mu a) \quad (24)$$

from Eq. (19) results in

$$k_s = \frac{R_s}{R_{E_1}} \left[\frac{\theta^{DR_m^S}(\mu a)}{\theta^{DR_m^{E_1}}(\mu a)} \right] k_{E_1} \quad (25)$$

Equation (25) expresses the relationship between the slopes of the calibration lines for the monoenergetic and polyenergetic plane sources.

Now if the calibration curves represented by Eqs. (20) and (21) are plotted on the same graph they would appear as illustrated in Figure 1. It should be noted that k_{E_1} is the slope corresponding to the dosimeter calibration curve for the monoenergetic plane source and k_s is the slope corresponding to the dosimeter calibration curve for the polyenergetic plane source.

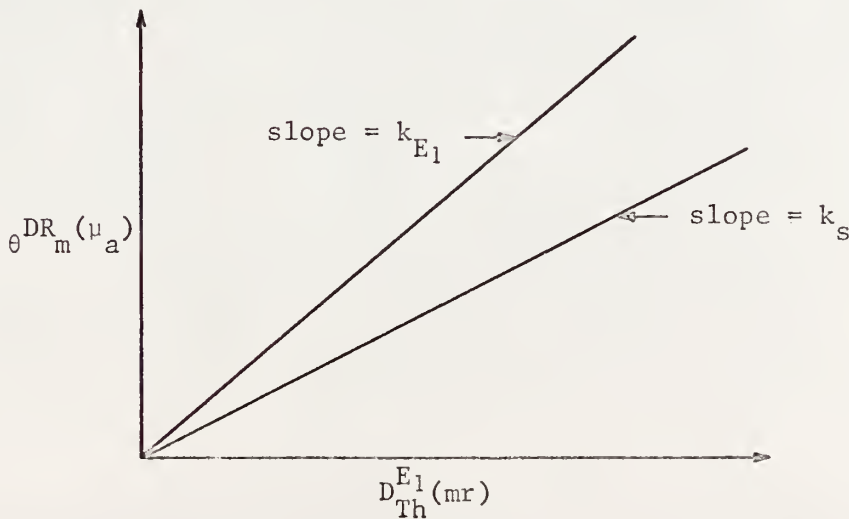


Figure 1. Dosimeter response versus exposure dose for exposure of a dosimeter to a monoenergetic plane source (slope = k_{E_1}) and a polyenergetic plane source (slope = k_s).

In representing these two curves graphically, the author has required that the product of the ratios (R_s/R_{E_1}) and $(\theta \mathcal{D}R_m^S(\mu a)/\theta \mathcal{D}R_m^{E_1}(\mu a))$ be less than unity as this is the case which will be encountered in this work.

Examination of this figure indicates that the two calibration curves are of the same form and in fact that they differ only with respect to their slopes. Referring to Eq. (25) it is apparent that the only difference in the slopes is that to obtain k_s from k_{E_1} a correction is necessary to account for the dependence of the collimator correction factor and the dosimeter response on the gamma-ray energy.

Therefore, using Eq. (19) and a monoenergetic plane source, it is possible to obtain a calibration curve for the dosimeter which will be suitable for use in the experiment described in Section 2.2. This calibration curve will correct for the energy response of the dosimeter as well as the effects of the collimator and thus will make possible the measurement of an exposure dose with the dosimeter which can be compared to that computed using the collimator-spectrometer system measurements and the unfolding technique.

3.0 EXPERIMENTAL APPARATUS

Experimental measurements were conducted at the Kansas State University Nuclear Engineering Shielding Facility on a 3500 square foot concrete slab. This slab was equipped with two fifty-foot towers located approximately sixty feet apart on one diagonal of the concrete slab.

A government surplus anti-aircraft searchlight which had been modified by removing the searchlight and replacing it by a 3500 pound lead collimator was used in the experimental measurements. The collimator housing was of such a design as to enable it to be used with either a blank collimator (no aperture) for background measurements or a two inch diameter by fourteen and one-half inch long collimator for differential dose measurements. This was possible through the insertion of the appropriate collimator into the collimator housing. The instrument cavity, located within the collimator, was in the form of a right circular cylinder with dimensions of three inches by thirteen and one-half inches. Copper tubing encircled the instrument cavity to allow preheated water to be forced through the collimator housing walls and thereby maintain the instrument cavity at a constant temperature. A Precision Scientific Company constant temperature circulating system was used to heat and force water at an elevated temperature through the copper tubing. A working drawing of the collimator system is shown in Figure 2.

A Harshaw integral line assembly, Type 12S12, was used in measuring the complex gamma-ray energy spectra. This assembly, consisting of a three inch by three inch cylindrical thallium-activated sodium-iodide crystal, photomultiplier tube, and associated parts, was used with a Hamner pre-amplifier, Model N-356. Power was supplied to the photomultiplier tube by

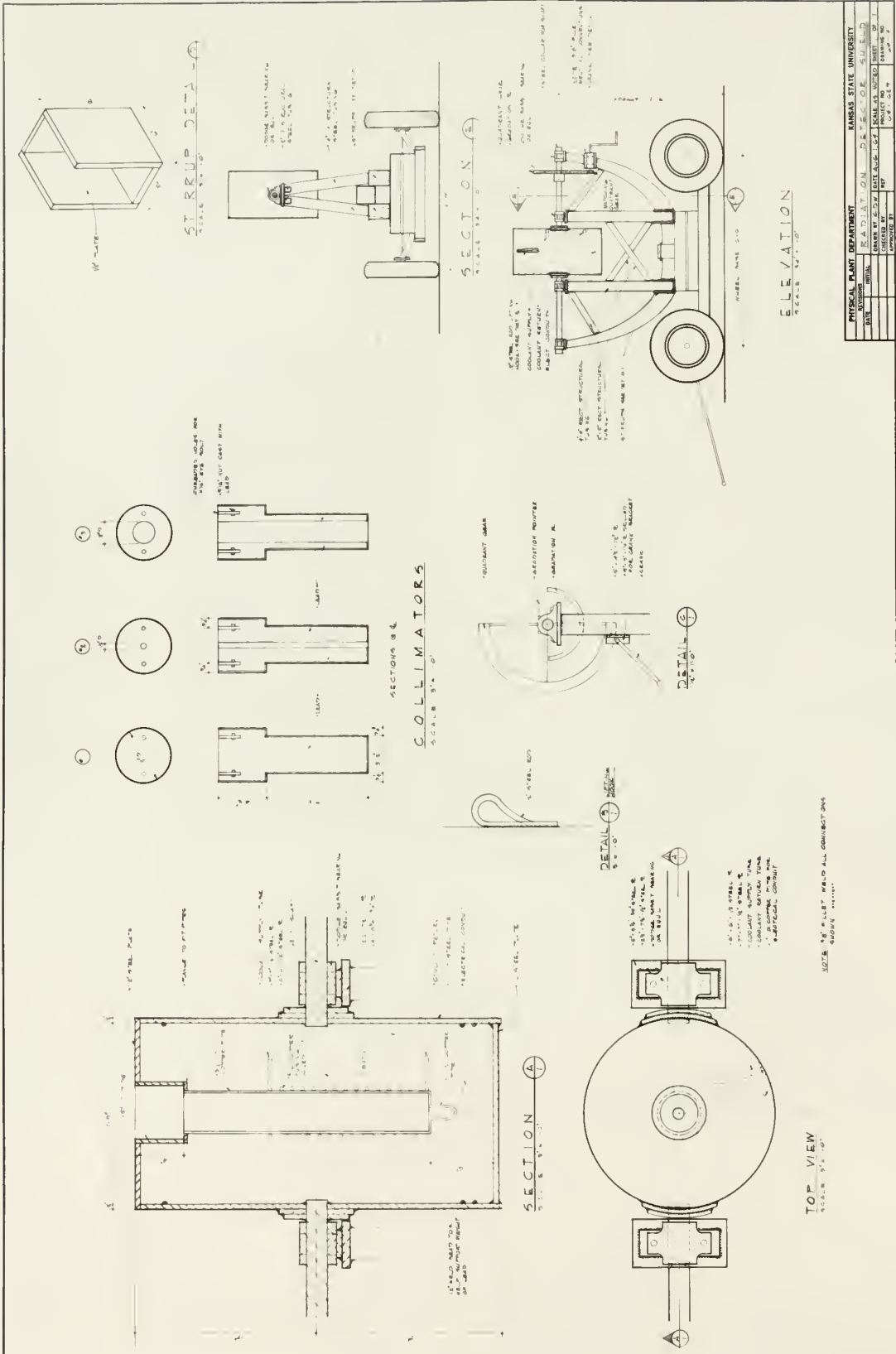


Figure 2. Machine drawing of the collimator system

a John Fluke Model 412A high voltage power supply. The preamplifier, which was driven by a Model HB2AM Kepco voltage regulated power supply, was capable of sending pulses from the photomultiplier tube through one thousand feet of signal cable. Pulses received from the preamplifier were analyzed using a Technical Measurements Corporation (TMC) multichannel analyzer system. This system consisted of a TMC Model 402-6 400 channel pulse-height analyzer and a TMC Model 520 type-punch-read control unit. The data accumulated by the multichannel analyzer system were read out using both a TMC Model 530 computer typewriter and a TMC 540R paper tape punch in conjunction with the type-punch-read control unit.

Dosimeter measurements were made using a Victoreen Instrument Company air equivalent stray radiation chamber, Model 239. This indirect reading dosimeter had a ten milliroentgen total dose capability and was read using a Technical Operations Incorporated dosimeter charger-reader. The integrated dose accumulated by the dosimeter was read on the charger-reader in terms of microamperes.

Two cobalt-60 sources of different strengths were used in making the required measurements. The use of two sources was necessary because of the differences in sensitivity of the dosimeter and the scintillation detector.

Measurements made with the scintillation detector used a Technical Operations Incorporated gamma-ray projector, Model 402, with a nominally 0.3 curie cobalt-60 source. (See reference 11.) This unit was operated by cranking the source out of its lead storage container by means of a flexible cable on the end of which the source was mounted. The flexible metallic hose through which the source was moved was equipped with an electrical control system (battery powered) so that the operator could determine when

the source was out of the storage container and when it was in position at the end of the metallic hose.

Dosimeter measurements were made using a Technical Operations Incorporated duplex hydraulic source circulation system, Model 539. In this system water was drawn from a fifty-five gallon reservoir through a high speed pump thereby applying pressure to the rear of a source piston assembly. A nominally ninety curie cobalt-60 source was mounted on this assembly. Thus the source was forced from its storage container into a length of polyethylene tubing which had been positioned to satisfy the requirements of the experimental configuration. By means of a forward and reverse switch the source could be positioned to within one inch of a selected location in the tubing. A detailed description of this source circulation system, with operating instructions, is contained in reference 12.

The calibration of the dosimeter in the collimator used a simulated plane source of cobalt-60. A uniform plane isotropic source of cobalt-60 was approximated by traversing a "line" source over a rectangular plane. The "line" source consisted of eighteen nominally four millicurie cobalt-60 sources. These sources were positioned on a cardboard holder by placing the small wire loop attached to the end of each source over one of the eighteen wire hooks located at one-half inch intervals along the length of the holder. This line source, which is illustrated in Figure 3, was then attached to the plane simulator shown in Figure 4 which traversed the line source in the horizontal and vertical directions simultaneously. The vertical speed was approximately one inch per minute and one complete revolution of the "line" source in the horizontal direction took about nineteen seconds. The plane simulator was capable of simulating an approximately twenty-eight inch square plane isotropic source of cobalt-60.

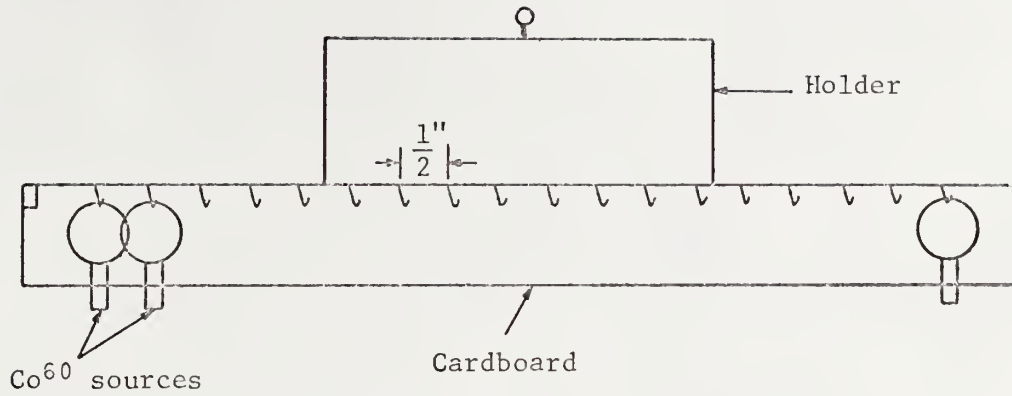


Figure 3. "Line" source consisting of eighteen cobalt-60 sources.

With regard to radiation safety, each person in the experimental area was equipped with a film badge, two pocket dosimeters and a radiation survey meter. Guards were employed to prevent the entry of unauthorized personnel to the experimental area. This was accomplished by having the guards constantly monitor the two milliroentgen per hour perimeter surrounding the experimental area while the experiments were in progress. In addition all experiments were carried out in accordance with the rules and regulations set forth by the Kansas State University Radiation Safety Committee and the appropriate state and federal licenses.

4.0 EXPERIMENTAL PROCEDURE

Polyenergetic gamma rays were obtained by scattering cobalt-60 radiation from a concrete slab. Two fifty foot towers were used to suspend a cobalt-60 source above the concrete slab. For selected scattering angles (see Figure 5) the collimator defined corresponding areas on the slab.

Experimental measurements were made using both the scintillation detector and the ten-milliroentgen-full-scale dosimeter. These detection instruments were positioned, one at a time, in the instrument cavity of the collimator and measurements were made for each of the experimental configurations to be considered. The geometry of the experimental configurations is illustrated in Figure 5. Each of these configurations was defined by the angles θ_0 , θ and ϕ as defined in this figure.

It should be noted that because of the design of the collimator the detector height for all measurements was maintained at five feet two inches. Also the source height above the concrete slab was held constant at ten feet.

For each experimental configuration and for both the scintillation detector and the dosimeter, a minimum of six measurements, three with the two inch collimator, and three using the blank collimator, were made to obtain a measure of the dose and background for the configuration under investigation. The geometry of each experimental configuration was reproduced independently at least three times for both the scintillation detector and dosimeter measurements. This was accomplished by making only one dose and background measurement for a particular experimental configuration before proceeding to the next one.

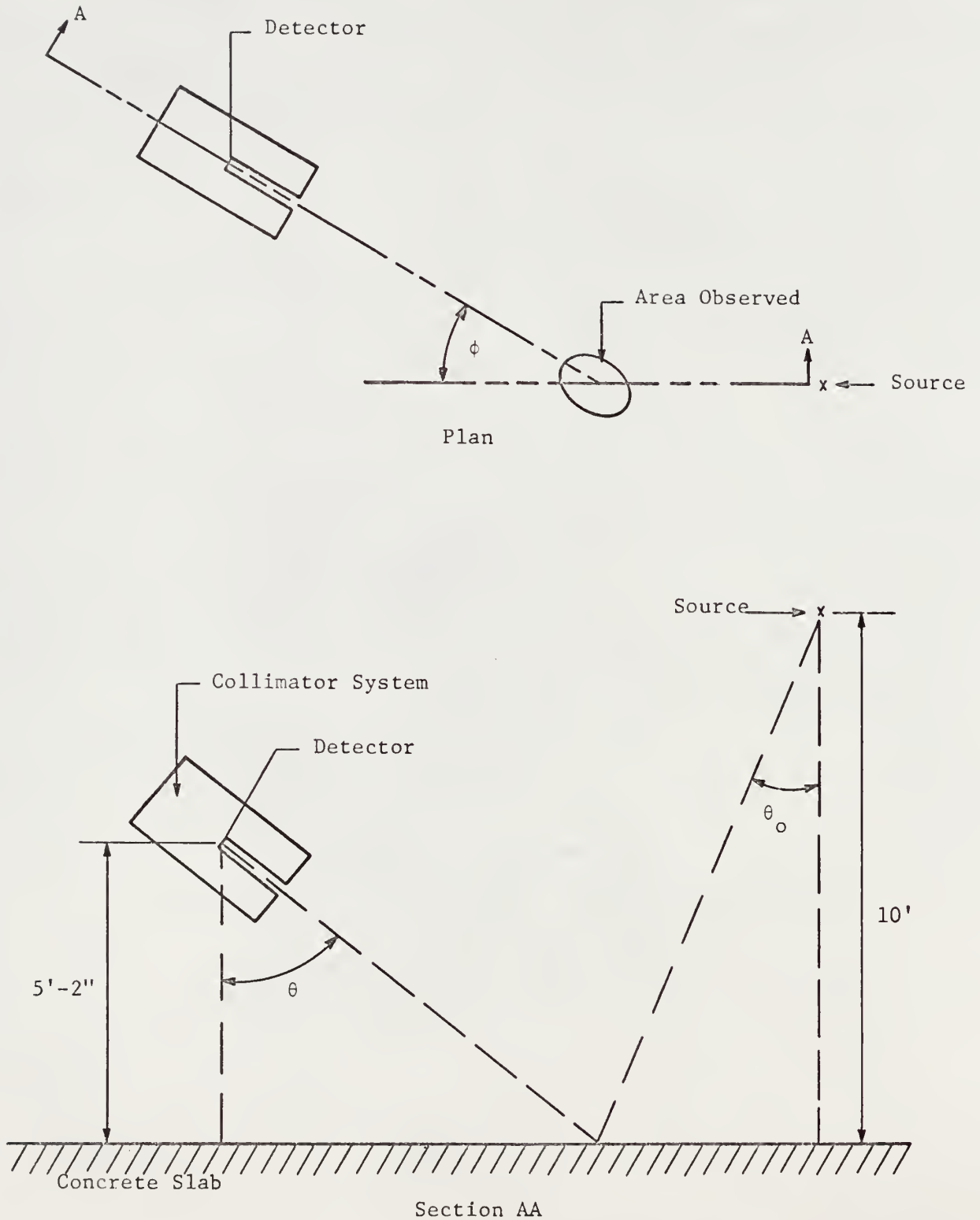


Figure 5. Experimental configuration used in the unfolding confirmation.

Spectral measurements were made using the sodium iodide scintillation detector and the Technical Operations gamma-ray projector with the nominally three-tenths curie cobalt-60 source. The source tip of the metallic hose of this unit was held in place above the concrete slab through the use of a rope from each of the fifty foot towers and guide wires to the concrete slab. For each measurement the collimator was positioned and the source was cranked from its storage container through the metallic hose to its position. Following the completion of the experimental run the source was returned to its storage container and preparations were made for the next measurement. A quality control program was developed to assure a consistent level of operation for the gamma-ray scintillation spectrometer system. This quality control program is presented in Appendix A.

The ten-milliroentgen full-scale dosimeter was calibrated using the "line" source and the plane simulator. The dosimeter was first positioned in the instrument cavity of the collimator so that the center of its active volume coincided with the axis of rotation of the collimator and its vertical axis coincided with the collimator axis. The calibration then consisted of measuring the dosimeter response for an exposure of one, two, three and four traversals of the line source over the prescribed plane. Figure 6 illustrates the experimental configuration for dosimeter calibration.

Measurements made with the ten-milliroentgen full-scale dosimeters were carried out using the Technical Operations Incorporated duplex hydraulic source circulation system with the nominally ninety curie cobalt-60 source. For these measurements the dosimeter was charged and put inside the collimator and then the collimator was positioned. The source was then pumped from its storage container into the polyethylene tubing and positioned using the forward and reverse switch on the pump console and a spotting

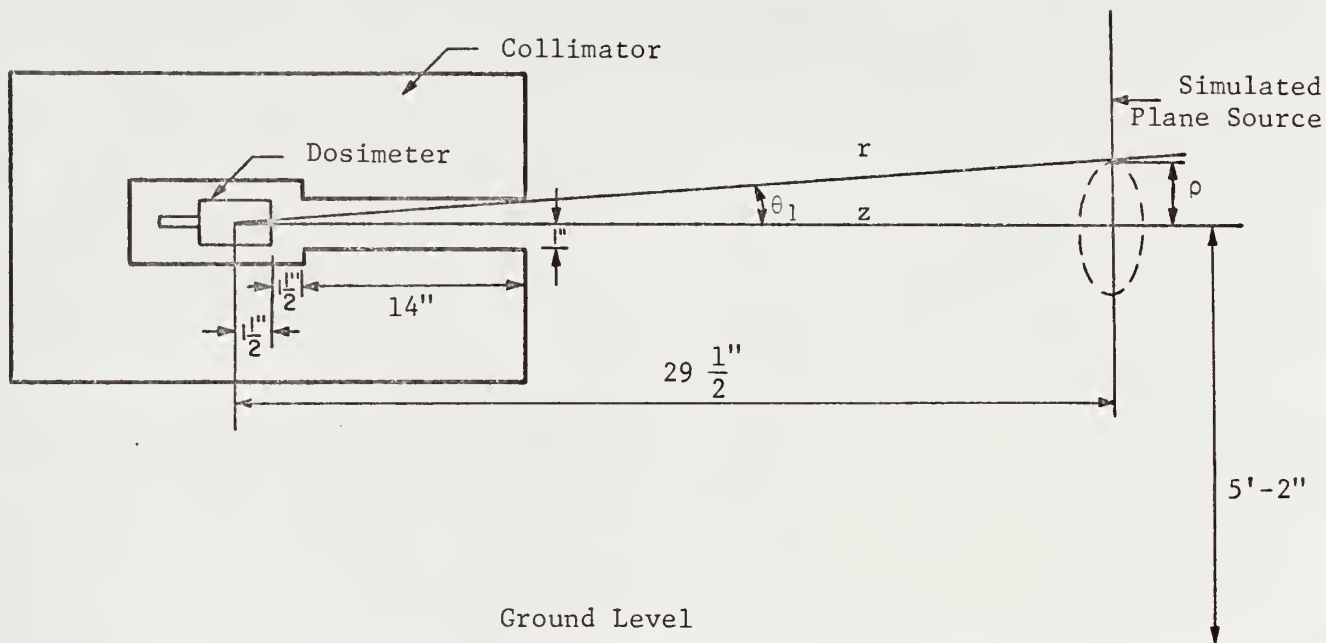


Figure 6. Experimental configuration for the dosimeter calibration

telescope. The tubing was positioned above the concrete slab by attaching it to a heavy wire support which was in turn suspended in air through the use of light ropes from the two fifty foot towers. Guide wires from the wire support to the concrete slab were used so that the tubing could be kept in a fixed position. At the end of a given experimental run the source was returned to its storage container and the dosimeter was then removed from the collimator and read using the Technical Operations Incorporated charger-reader.

Before the dosimeter calibration equations could be determined it was first necessary to calibrate the cobalt-60 simulated plane source in the manner described in Appendix B. This determination of the cobalt-60 simulated plane source strength required that first the dosimeter be calibrated using a calibrated cobalt-60 point source (Appendix C).

Since this work contains a number of different experiments, some of which are dependent on others, the experiments and calculations performed during the course of this work are illustrated in schematic form in Figure 7.

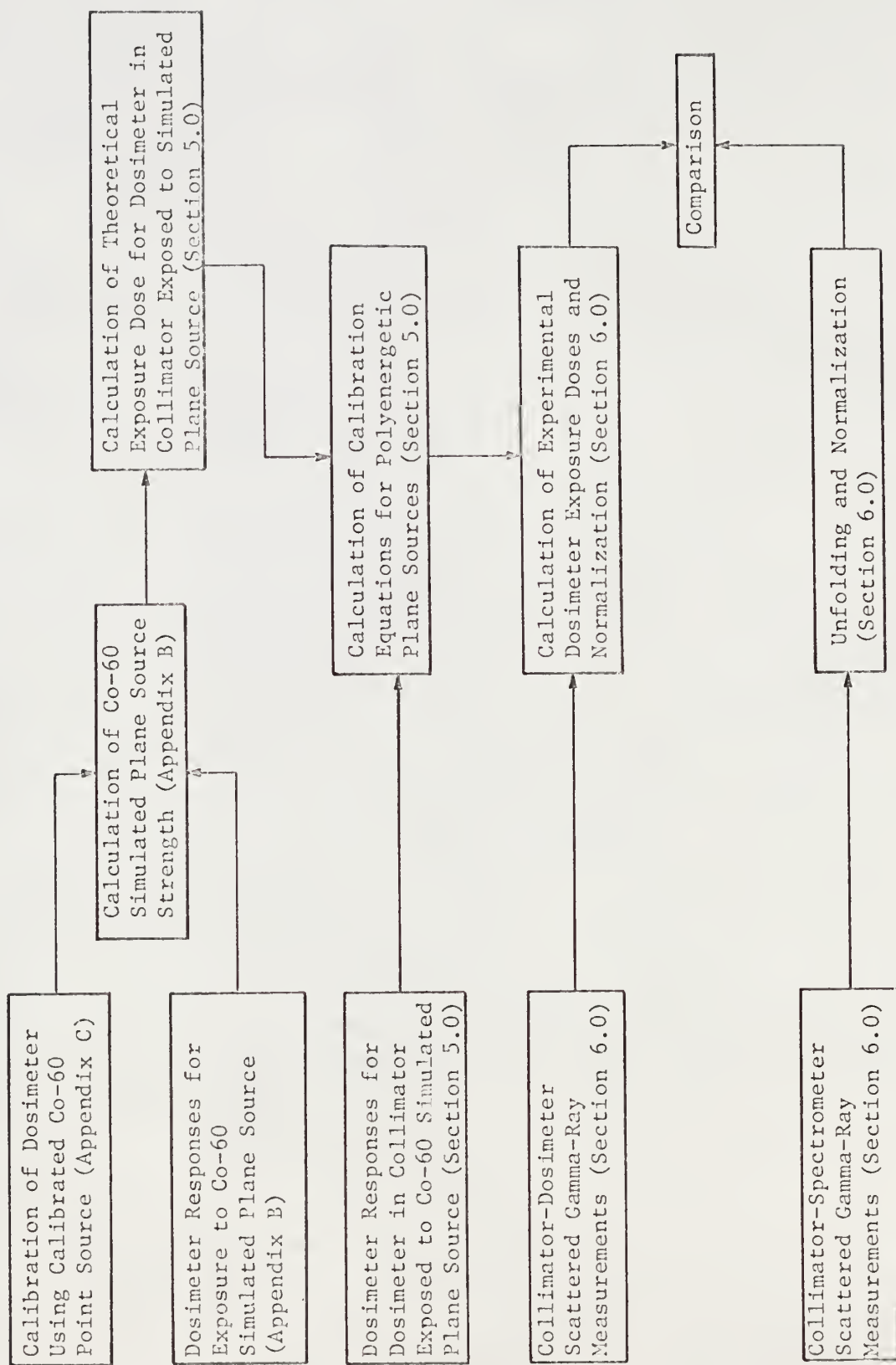


Figure 7. Schematic of experiments and calculations performed in the confirmation of the unfolding codes

5.0 CALIBRATION OF THE DOSIMETER
LOCATED WITHIN THE COLLIMATOR

The ten-milliroentgen total-dose dosimeter was calibrated with the dosimeter located at the center of the collimator. As a result of the calibration measurements made, equations for the calibration curves could be computed which would be suitable for use in the dosimeter measurements of the scattered gamma-ray energy distributions considered in Section 1.2. These calibration curves are based on Eq. (19), i.e.,

$$\theta_{DR_m^S}(\mu a) = \frac{R_s}{R_{E1}} \left[\frac{\theta_{DR_m^S}(\mu a)}{\theta_{DR_m^{E1}}(\mu a)} \right] \theta_{DR_m^{E1}}(\mu a) = \frac{R_s k_s}{\alpha_\theta} D_{Th}^{E1}(\text{mr}) ,$$

which was derived in Section 1.3.

This calibration experiment consisted of measuring the response of the dosimeter, located within the collimator, exposed to the simulated plane isotropic source of cobalt-60. The geometry for these measurements is illustrated in Figure 6 and the "line" source and plane simulator used in simulating the plane isotropic source of cobalt-60 are illustrated in Figures 3 and 4 respectively. Dosimeter responses were measured for one, two, three and four simulations of the plane source. These measured dosimeter responses, in microamperes, were corrected for temperature and pressure using Eq. (C-1) of Appendix C and normalized to a twenty-eight minute simulation of the plane source. These corrected dosimeter responses correspond to $\theta_{DR_m^{E1}}(\mu a)$ in Eq. (19).

The theoretical dose, $D_{Th}^{E1}(\text{mr})$ in Eq. (19), corresponding to the experimental measurements described above was based on the dose which would be expected at the center of the dosimeter due to one simulation of the plane

source of cobalt-60. Thus using the strength of the simulated plane source as determined in Appendix B the theoretical dose can be calculated from

$$D_{Th}^{E1}(\text{mr}) = \iint_A \frac{D_p}{4\pi r^2} d^2A, \quad (26)$$

where D_p = strength of the plane source in milliroentgens per twenty-eight minutes,*

A = area, in square centimeters, on the plane source defined by the solid angle of the collimator,

r = the distance in centimeters from the differential area d^2A to the center of the collimator.

Recognizing that $d^2A = 2\pi\rho d\rho$, $r = z \sec \theta$ and $\rho = z \tan \theta$, then a change of variable from ρ to θ in Eq. (26) yields

$$D_{Th}^{E1}(\text{mr}) = \int_0^{\theta_1} 1/2 D_p \tan\theta d\theta = 1/2 D_p (-\ln(\cos\theta_1)) \quad (27)$$

in which θ_1 , ρ and z are defined in Figure 6. Substitution of the appropriate value for θ_1 yields

$$D_{Th}^{E1}(\text{mr}) = 8.66 \times 10^{-4} D_p \quad (28)$$

or

$$D_{Th}^{E1}(\text{mr}) = 0.568 \pm 0.014 \quad (29)$$

* Although D_p , which could not be measured experimentally, has the units of dose, it actually represents the product of source strength, exposure time and the flux to dose conversion factor. This unusual term was employed for convenience in carrying out the calculations.

where the value for D_p was obtained from the calibration of the plane source (see Appendix B). Thus Eq. (29) represents the expected dose per simulation of the plane source due only to those gamma-rays which leave the plane source in such a direction as to strike the detector without the need of an intermediate scatter.

It was noted in Section 2.3 that the evaluation of the ratios (R_s/R_{E_1}) and $(\mathcal{D}R_m^S(\mu a)/\mathcal{D}R_m^{E_1}(\mu a))$ requires a knowledge of the scattered gamma-ray energy distributions for which the calibration curves are to be applicable. Also in this previous discussion, it was stated that since only the average energy of the gamma-ray energy distribution was necessary for the evaluation of these two ratios, the single scattered energy based on the experimental geometry could be used to approximate the average energy of each experimental configuration. However, in evaluating this approximation it is first necessary to consider how the dosimeter response and the collimator correction factor vary with gamma-ray energy.

The problem of collimator effects has been examined on a theoretical basis by Mather (13) and experimentally by Tomnovec and Mather (14). In both of these papers results have been given relating the ratio of collimator-interacted radiation to direct radiation (this corresponds to $R - 1.0$ as defined in this report) at some point within the collimator to the energy of the gamma rays incident on the face of the collimator. From these studies it can be seen that the collimator correction factor R can be very closely approximated as a linear function of gamma-ray energy. This approximation will not introduce an error of more than five percent in the value of $(\mathcal{D}R_m^S(\mu a)/\mathcal{D}R_m^{E_1}(\mu a)) \rightarrow R_s/R_{E_1}$.

If R is assumed to be a linear function of gamma-ray energy, all that is needed to relate R and the gamma-ray energy are two points. One point on a curve of R versus gamma-ray energy is the point (1.000, 0.00). This point follows directly from the definition of R and from the fact that the absorption cross section for lead at low energies greatly outweighs the Compton cross section and that the linear attenuation coefficient increases rapidly for decreasing gamma-ray energy. The value of R_{E_1} can be calculated from the experimental measurements made using the plane source and knowing the strength of the simulated plane source. Hence it is found that $R_{E_1} = 1.677$ and therefore the second point is (1.677, 1.25) where 1.25 is the average energy in MeV of the two gamma rays emitted by cobalt-60. Using these two points then the slope of the line can be computed and the resulting expression relating the collimator correction factor R to the incident gamma-ray energy E is

$$R = 1.000 + 0.542 E . \quad (30)$$

The ratio $(\frac{\partial R_m^S(\mu a)}{\partial R_m^{E_1}(\mu a)})$ can be obtained directly from a curve (15) of dosimeter response at an energy E , relative to the response to cobalt-60 radiation versus gamma-ray energy. This curve indicates that the variation of the dosimeter response relative to its response to cobalt-60 radiation is nearly constant for decreasing gamma-ray energies down to approximately 0.2 MeV.

Based on this analysis of the energy dependence of the ratios (R_S/R_{E_1}) and $(\frac{\partial R_m^S(\mu a)}{\partial R_m^{E_1}(\mu a)})$, it is possible to predict the error introduced through the use of the single scattered energy as the average energy of the gamma-ray energy distribution under investigation. Since the ratio

$(\frac{\partial R_m^S}{\partial \mu a}) / (\frac{\partial R_m^{E_1}}{\partial \mu a})$ is essentially a constant for gamma-ray energies down to approximately 0.2 MeV, then as long as the average energy is sufficiently larger than this lower limit an error incurred through the use of the single scattered energy will affect this ratio negligibly. The ratio (R_s/R_{E_1}) , however, is sensitive to an error in the average energy used. As an example if the single scattered energy calculated is a factor of two larger than the true average energy of the scattered gamma-ray energy distribution the error introduced in the ratio (R_s/R_{E_1}) will be approximately ten percent.

The single scattered energy approximation is an upper limit to the average energy of the gamma rays reaching the detector after scattering from the concrete. This follows from the fact that a significant fraction of the gamma rays striking the detector have suffered multiple collisions in the concrete. These multiply scattered gamma rays will have a much lower energy and thus it is obvious that the true average gamma-ray energy of the concrete scattered radiation will be less than the single scattered energy and that the single scattered energy will be an upper limit.

Now the single scattered energy E_{ss} , for each of the experimental configurations being considered, can be computed from

$$E_{ss} = \frac{E_1}{1.0 + \frac{E_1(1.0 - \cos \theta_s)}{m_0 c^2}} \quad (31)$$

where E_1 = incident gamma-ray energy on the concrete, 1.25 MeV average for cobalt-60,

$m_0 c^2$ = rest energy of an electron, 0.51 MeV, and

$\cos \theta_s$ = cosine of the scattering angle θ_s .

The cosine of the scattering angle can be computed using

$$\cos \theta_s = -\sin \theta_0 \sin \theta \cos \phi + \cos \theta_0 \cos \theta \quad (32)$$

where the angles θ_0 , θ and ϕ are defined in Figure 5.

Thus the single scattered gamma-ray energy for each of the experimental configurations can be determined using Eqs. (31) and (32). The experimental configurations, designated as P_1 , P_2 and P_3 , and their defining angles θ_0 , θ and ϕ along with the single scattered energies for each are listed in Table I.

Table I. Experimental configurations and corresponding energies of once scattered gamma rays

Experimental Configuration	Defining angles in degrees			E_{ss} (MeV)
	θ_0	θ	ϕ	
P_1	00.0	72.0	00.0	0.295
P_2	41.4	72.0	00.0	0.505
P_3	60.0	72.0	52.5	0.481

Using the single scattered energies as presented in Table I, the values of $(\mathcal{D}R_m^S(\mu a)/\mathcal{D}R_m^{E_1}(\mu a))$ and R_s can be determined in the manner previously described. Hence with the value of R_s and the previously calculated value of R_{E_1} the ratio (R_s/R_{E_1}) can be evaluated for each of the experimental configurations. The values of these ratios for each of the experimental configurations are presented in Table II.

Table II. Values of (R_s/R_{E_1}) and $(\frac{\partial DR_m^S(\mu a)}{\partial DR_m^{E_1}(\mu a)})$ for each experimental configuration based on energies of once scattered gamma rays

Experimental configuration	$\frac{R_s}{R_{E_1}}$	$\frac{\frac{\partial DR_m^S(\mu a)}{\partial DR_m^{E_1}(\mu a)}}{\frac{\partial DR_m^{E_1}(\mu a)}{\partial DR_m^{E_1}(\mu a)}}$
P ₁	0.692	0.993
P ₂	0.759	0.989
P ₃	0.752	0.992

With the values given in the above table, the experimentally measured dosimeter responses, $\frac{\partial DR_m^{E_1}(\mu a)}{\partial DR_m^{E_1}(\mu a)}$, and the theoretical doses, $D_{Th}^{E_1}(\text{mr})$, from Eq. (29), the equation of the calibration curve can be calculated for each of the three experimental configurations. This is accomplished through the application of the regression analysis of Appendix D to Eq. (19). This application involves considering x as $D_{Th}^{E_1}(\text{mr})$ and y as the product $(R_s/R_{E_1}) (\frac{\partial DR_m^S(\mu a)}{\partial DR_m^{E_1}(\mu a)}) \frac{\partial DR_m^{E_1}(\mu a)}{\partial DR_m^{E_1}(\mu a)}$.

As an example, the determination of the equation for the calibration curve for the P₁ experimental configuration is presented below. The experimental dosimeter responses $\frac{\partial DR_m^{E_1}(\mu a)}{\partial DR_m^{E_1}(\mu a)}$, corrected for temperature and pressure, the product $(R_s/R_{E_1}) (\frac{\partial DR_m^S(\mu a)}{\partial DR_m^{E_1}(\mu a)}) \frac{\partial DR_m^{E_1}(\mu a)}{\partial DR_m^{E_1}(\mu a)}$ and $D_{Th}^{E_1}(\text{mr})$ are listed in Table III for one, two, three and four simulations of the plane source of cobalt-60. The last two columns in this table represent y and x respectively as used in the regression analysis which follows.

Table III. Data used to determine the equation of the calibration line for the P₁ configuration

Simulations of Plane Source	$\theta_{DR_m^{E_1}}(\mu a)$	$\left(\frac{R_s}{R_{E_1}}\right) \left(\frac{\theta_{DR_m^S}(\mu a)}{\theta_{DR_m^{E_1}}(\mu a)}\right)$	$\theta_{DR_m^{E_1}}(\mu a)$	$D_{Th}^{E_1}(\text{mr})$
1	8.40		5.78	0.568 ± 0.014
	7.83		5.38	
	8.38		5.76	
	8.23		5.66	
2	15.58		10.71	1.137 ± 0.028
	15.66		10.77	
	15.55		10.69	
	16.11		11.08	
3	22.63		15.56	1.705 ± 0.042
	23.49		16.15	
	23.38		16.08	
	23.70		16.30	
4	31.37		21.56	2.272 ± 0.056
	31.54		21.69	
	30.90		21.25	

Since the x values ($D_{Th}^{E_1}(\text{mr})$) in Table III have a constant percentage error, the equation of the calibration line can be determined using the regression analysis for a controlled experiment as outlined in Appendix D. The slope of the line is

$$b = \frac{\sum_{i=1}^{15} x_i y_i}{\sum_{i=1}^{15} (x_i)^2} = 9.46 \quad (33)$$

The estimate of σ^2 , from Eq. (D-20) of Appendix D, is

$$(s')^2 = s^2 + b^2 V[x] \quad (34)$$

or

$$(s')^2 = \frac{\sum_{i=1}^{15} (y_i)^2 - [(\sum_{i=1}^{15} x_i y_i)^2 / \sum_{i=1}^{15} (x_i)^2]}{\ell - 1} + b^2 V[x] \quad (35)$$

where $V[x]$ is the variance on x and $(\ell-1)$ represents the degrees of freedom.

Substitution of the appropriate values yields

$$s' = [0.0688 + b^2(0.0251 x)^2]^{1/2} . \quad (36)$$

However, the calibration line is to be used in reverse to convert a measurement in microamperes to an exposure dose in milliroentgens. Therefore using Eq. (D-21) of Appendix D, the value of x can be determined for \bar{y}' , the mean of m new observations. The form of this equation is

$$x = \frac{\bar{y}'}{b} \pm \frac{t s'}{b} \left[\frac{1}{m} + \frac{(\bar{y}')^2}{b^2 \sum_{i=1}^{15} (x_i)^2} \right]^{1/2} \quad (37)$$

if g' , as defined by Eq. (D-22) of Appendix D, is less than 0.1. Substitution of the appropriate values into the expression for g' indicate that, in the range of interest, g' is less than 0.1. Thus Eq. (37) is a valid representation for the regression line in reverse. Recognition that x in Eq. (36) can be replaced by \bar{y}'/b , substitution of the proper values into Eq. (37) yields

$$x = \frac{\bar{y}'}{9.46} \pm \frac{(1.034)[0.0688 + (0.0251 \bar{y}')^2]^{1/2}}{9.46} \left[\frac{1}{m} + \frac{(\bar{y}')^2}{(9.46)^2(33.60)} \right]^{1/2} \quad (38)$$

where the value of t for 68 percent confidence and fourteen degrees of freedom is 1.034.

In the interest of clarity the equation of the calibration line can be written in terms of the experimental parameters by replacing x by $D_{Th}^{E_1}(mr)$ and \bar{y} by $\overline{\theta DR_m^S(\mu a)}$ which from Eq. (19) is equal to the product term $(R_s/R_{E_1}) [\overline{\theta DR_m^S(\mu a)}/\overline{\theta DR_m^{E_1}(\mu a)}] \overline{\theta DR_m^{E_1}(\mu a)}$. Thus Eq. (38) can be written as

$$D_{Th}^{E_1}(mr) = \frac{\overline{\theta DR_m^S(\mu a)}}{9.46} + \frac{(1.034)[0.0688 + (0.0251 \overline{\theta DR_m^S(\mu a)})^2]^{1/2}}{9.46} \left[\frac{1}{m} + \frac{(\overline{\theta DR_m^S(\mu a)})^2}{(9.46)^2(33.60)} \right]^{1/2} \quad (39)$$

where $\overline{\theta DR_m^S(\mu a)}$ is the mean of m new observations. Equation (39) represents the calibration line for the P_1 experimental configuration. By replacing the values of $(R_s/R_{E_1}) (\overline{\theta DR_m^S(\mu a)}/\overline{\theta DR_m^{E_1}(\mu a)}) \overline{\theta DR_m^{E_1}(\mu a)}$ in Table III by their corresponding values for the P_2 and P_3 configurations, the equations representing these calibration lines for these configurations can be obtained in a similar manner. Hence the equation of the calibration line for the P_2 experimental configuration is

$$D_{Th}^{E_1}(mr) = \frac{\overline{\theta DR_m^S(\mu a)}}{10.33} + \frac{(1.034)[0.0823 + (0.0251 \overline{\theta DR_m^S(\mu a)})^2]^{1/2}}{10.33} \left[\frac{1}{m} + \frac{(\overline{\theta DR_m^S(\mu a)})^2}{(10.33)^2(33.60)} \right]^{1/2} \quad (40)$$

and for the P_3 configuration the equation is

$$D_{Th}^{E_1}(mr) = \frac{\overline{\theta DR_m^S(\mu a)}}{10.26} + \frac{(1.034)[0.0811 + (0.0251 \overline{\theta DR_m^S(\mu a)})^2]^{1/2}}{10.26} \left[\frac{1}{m} + \frac{(\overline{\theta DR_m^S(\mu a)})^2}{(10.26)^2(33.60)} \right]^{1/2} \quad (41)$$

6.0 DISCUSSION OF RESULTS

The experimental measurements were carried out using the experimental configuration illustrated in Figure 5 and the procedure outlined in Section 4.0. Three different configurations, obtained by varying θ_0 and ϕ were investigated. The three experimental configurations examined were designated as P_1 , P_2 and P_3 and correspond to combinations of the angles θ_0 , θ and ϕ as shown in Table I. Measurements were made using the scintillation detector system and the ten milliroentgen dosimeter alternately in the lead collimator. These measurements utilized both the two-inch and the blank collimators.

The experimentally observed gamma-ray energy spectra were obtained using the scintillation detector and the nominally ninety curie cobalt-60 source. A consistent level of operation of the scintillation detector and the pulse-height analyzer was obtained through the use of the quality control program presented in Appendix A.

Gamma-ray spectra obtained for each of the experimental configurations using the two-inch collimator were averaged and normalized to an exposure time of one hour. The corresponding blank collimator measurements were also averaged and normalized to a one hour exposure time. The two averaged spectra for each experimental configuration were then differenced and put into twenty-five energy bins of forty-eight keV per bin. These binned spectra were then used as input to the unfolding codes discussed in Section 1.1. The output from the unfolding codes was the unfolded pulse-height distribution \bar{N} . The averaged and differenced experimental spectra and their corresponding unfolded pulse-height distributions are illustrated in Figures 8, 9 and 10.

With reference to Figures 8, 9 and 10, in both the original spectra and the unfolded pulse-height distributions, three peaks are clearly discernable.

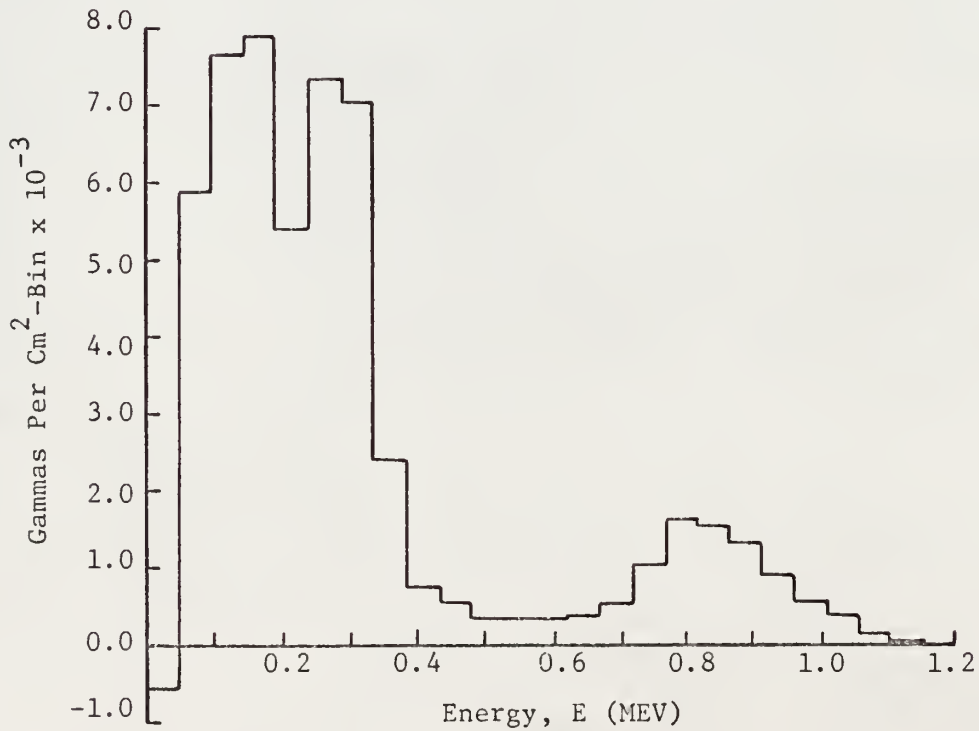
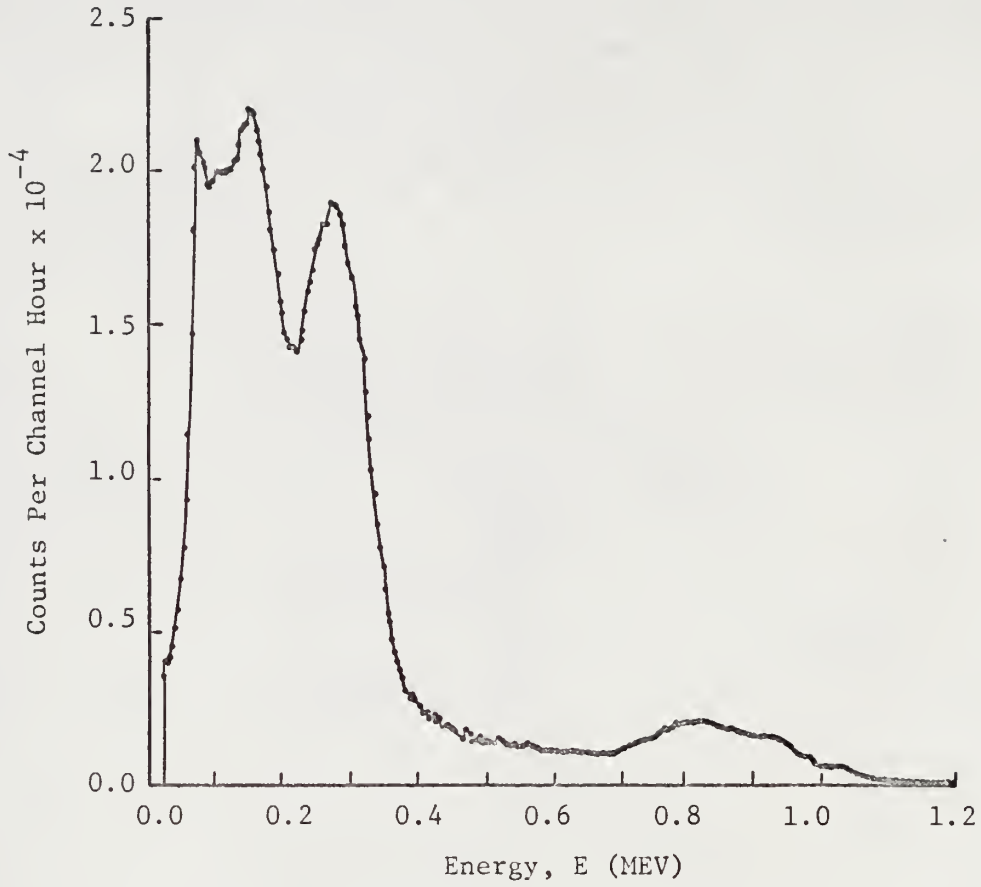


Figure 8. Original and unfolded spectra for the P_1 configuration

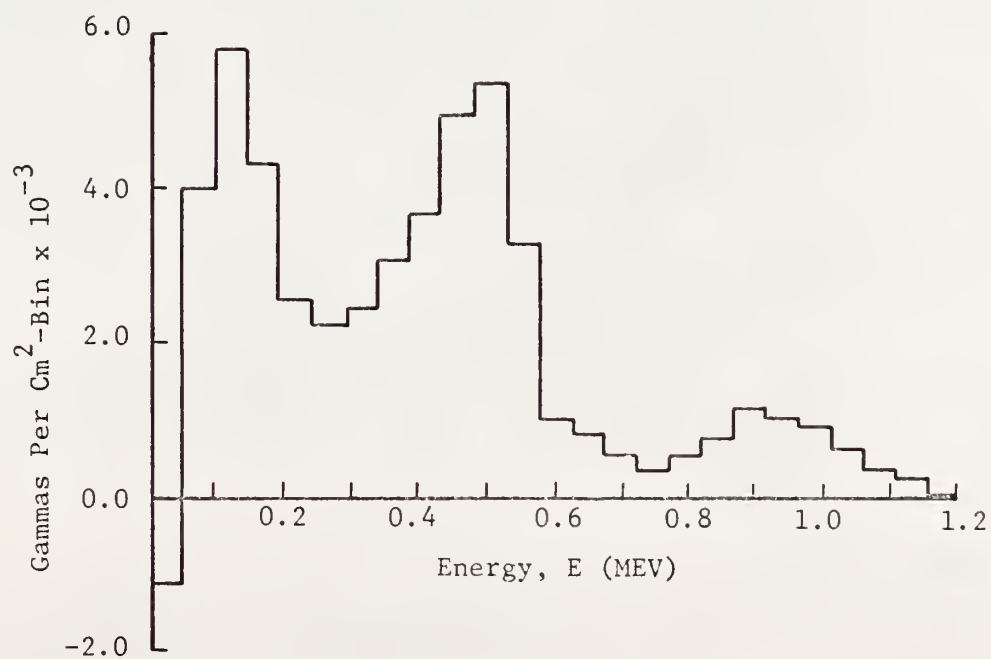
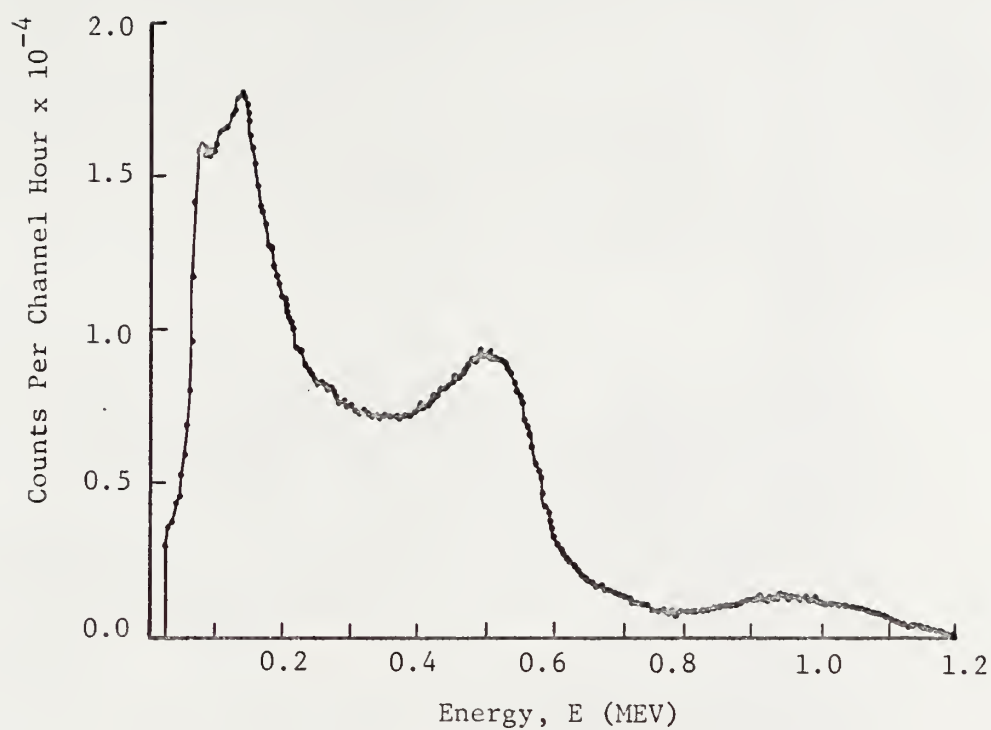


Figure 9. Original and unfolded spectra for the P_2 configuration

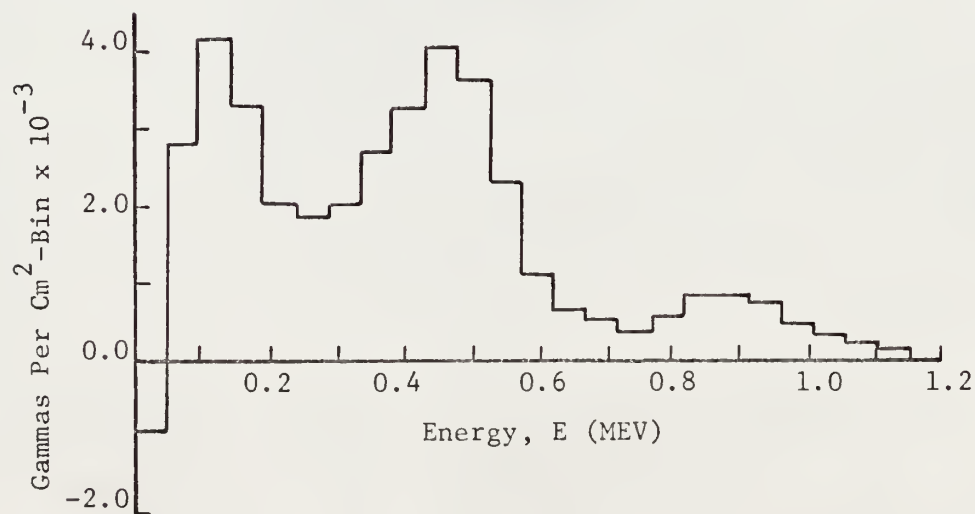
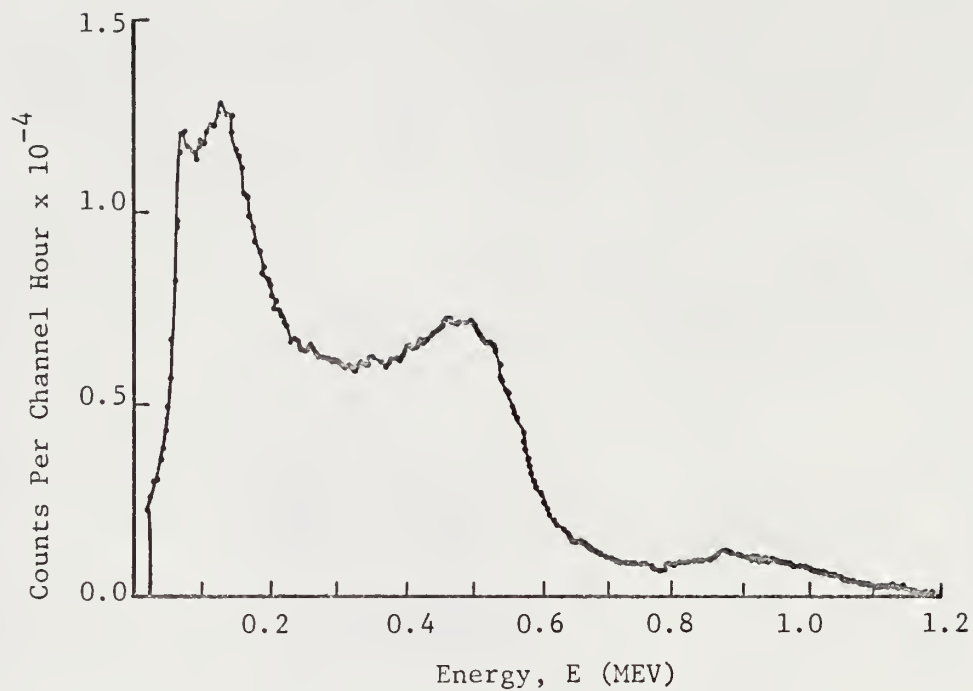


Figure 10. Original and unfolded spectra for the P_3 configuration

The lowest energy peak is due to gamma rays which were multiple scattered in the concrete and the middle peak corresponds to the single scattered gamma rays. The small peak at an energy of approximately nine-tenths of an MeV corresponds to those gamma rays which were singly scattered from the lip of the collimator. Upon examination it is found that there is close agreement between the concrete single scattered peak energies (energy corresponding to the middle peak in each spectrum) and the single scattered energies presented in Table I.

It should be noted that the contribution to the pulse-height distribution from the first energy bin in Figures 8, 9 and 10 is negative. Although these negative contributions, which correspond to negative fluxes, are not consistent with physical reality they must be considered when the exposure doses for each of the unfolded pulse-height distributions are computed. This results from the fact that the objective of this report is to determine how accurate the unfolding technique of Baran (10) is when used to compute exposure doses rather than a detailed analysis of the unfolding technique.

Even though a detailed analysis of the unfolding technique is not within the immediate objectives of this work, an indication as to the source of this error is in order. The lowest energy source used in the calibration of the spectrometer system was cobalt-60 metastable which emits gamma rays with energies of 58.9 keV. Since the first energy bin covers the energy range from 0.0 to 48.0 keV, then the development of the response matrix required an extrapolation of the experimental data to obtain a response function corresponding to this first energy bin. A linear extrapolation was used in developing the response matrix for the unfolding technique considered in this work (10). However, such a linear extrapolation does not appear to be

consistent with the interaction processes of low energy gamma rays with the scintillation detector and in fact such a linear extrapolation results in an overestimation of the gamma-ray contribution in the response function corresponding to the first energy bin. This problem is being considered in detail by Baran (16).

The unfolded pulse height distributions having units of gamma rays per square centimeter per hour were converted to exposure doses using

$$D = G \sum_{i=1}^{25} N_i E_i (\mu_a(E_i)/\rho)_{\text{air}} \quad (42)$$

where D = exposure dose in mr/hr,

G = conversion factor, 1.91×10^{-5} (mr-gm/MeV),

N_i = number of gamma rays per square centimeter per hour in the i th energy bin and

$\left(\frac{\mu_a(E_i)}{\rho}\right)_{\text{air}}$ = gamma-ray energy absorption mass attenuation coefficient (cm²/gm) corresponding to the energy E_i .

The error associated with each of these exposure doses was determined using an error analysis derived by Baran (10). This analysis considers both the errors in the experimental measurements and those introduced by the experimentally determined response matrix as well as the error introduced by the unfolding process itself.

Dosimeter measurements were made by replacing the scintillation detector by the ten-milliroentgen total-dose dosimeter. The same experimental configurations were investigated in these measurements as were examined using the scintillation detector. However, because of the relative sensitivities of the two detection instruments, the nominally ninety curie cobalt-60

source was employed in these measurements. A minimum of three measurements were made for each configuration using the two-inch collimator. Following a series of measurements utilizing the blank collimator it was concluded that the background was negligible. This conclusion was further verified by theoretical calculations.

Experimentally measured dosimeter responses, in microamperes, were corrected for temperature and pressure using Eq. (C-1) of Appendix C and then averaged for each of the experimental configurations. The average response was then substituted into the appropriate equation of the calibration line (Eq. 39, 40 or 41) corresponding to the experimental configuration under consideration to obtain the exposure dose. These doses, one for each configuration, were then normalized to a one hour exposure time.

In order that a meaningful comparison could be made between the exposure doses measured using these two methods, a correction was necessary to account for the difference in the strength of the sources used in the scintillation detector and dosimeter measurements. This adjustment was made by normalizing the exposure doses to a source strength of one curie. Thus the exposure doses obtained from the unfolding codes and the dosimeter measurements were divided by 0.243 ± 0.007 and 82.6 ± 1.8 curies respectively. These source strengths were obtained by correcting the calibrated strengths of these sources for the decay in their strengths which had occurred from the date they were calibrated to the date when they were used in making these measurements. These normalized exposure doses in mr per hour per curie, are presented in Table IV for each of the experimental configurations considered. In this table the doses obtained as a result of the application of the unfolding technique to the complex spectra observed are designated as the

Table IV. Comparison of spectral and dosimeter exposure doses

Experimental Configuration	Spectral Dose (mr/hr-curie)	Dosimeter Dose (mr/hr-curie)	Percentage Error
P ₁	0.0375 ± 0.0081	0.0264 ± 0.0008	42.0
P ₂	0.0451 ± 0.0061	0.0291 ± 0.0009	55.0
P ₃	0.0350 ± 0.0048	0.0240 ± 0.0007	45.8

spectral doses. The spectral dose is equivalent to D obtained from Eq. (36) normalized to a one curie source strength. The per cent error is equal to 100% (spectral dose - dosimeter dose)/dosimeter dose.

The results presented in Table IV indicate an average percentage difference between the spectral and dosimeter doses of 47.6 per cent. The percentage error on the individual doses ranged from 13.5 to 21.6 per cent for the spectral doses and from 2.9 to 3.0 per cent for the dosimeter doses. These individual errors are an indication of the precision with which the experimental measurements were made and the error introduced in reducing the experimental data.

It should also be noted that the difference between the spectral and dosimeter doses is such that the magnitudes of these two doses are not within one standard deviation of each other. Therefore it is apparent that there is an error in one or both of the methods used to determine the exposure doses presented in Table IV. Since the range of the percentage errors given in Table IV is not large it is not unreasonable to suspect that the error is systematic.

At this point it must be recalled that one of the primary objectives of this work was to determine the accuracy of the unfolding technique. To achieve this goal it was pointed out (see Section 2.2) that first the accuracy of the dosimeter results must be established. Thus the validity of the method used to calculate the exposure doses from the dosimeter data must be confirmed. In addition, estimates of the errors associated with any of the approximations used in determining the dosimeter doses should be obtained. If it can be shown that the dosimeter doses presented in Table IV were obtained by a valid method and that they are accurate, within some maximum error limit, then the case where there is not an overlap between this maximum error limit on the dosimeter doses and the error limit on the spectral doses would indicate that the spectral doses were in error. Therefore an estimation of the errors associated with the approximations used in obtaining the dosimeter calibration equations as well as a detailed discussion concerning the validity of these calibration equations is given in the following paragraphs.

The dosimeter doses presented in Table IV are almost entirely dependent on the equations for the calibration curves as developed in Section 5.0. In the development of these curves, two approximations were made: (1) that the average energy of the gamma-ray distribution could be approximated by the single scattered energy of the gamma rays scattered from the concrete surface and (2) that the curve of the collimator correction factor R versus gamma-ray energy could be represented by a straight line. Considering the first of these assumptions it was previously stated that the single scattered energy would be higher than the average energy, but that this overestimation would result in an error of no more than ten per cent. The second assumption

could result in an error of approximately five per cent as previously stated in Section 5.0. Both of these errors together could then possibly increase the confidence limits on the dosimeter doses by as much as 15 per cent.

The previous discussion would tend to indicate that if appropriate corrections had been made for the collimator interactions, as pertains to the dosimeter measurements, that the dosimeter and spectral doses would be in closer agreement. However, upon closer examination of the equations for the calibration curves it can be found that this is not the case. The validity of this statement becomes apparent when no corrections are made for the collimator interactions, i.e., letting $(R_s/R_{E_1}) = 1.0$ in Eq. (19). If the calibration equations of Section 5.0 are developed under this condition the average percentage difference between the spectral and dosimeter doses is 20 per cent and the spectral doses still have the contribution due to collimator interactions removed. Going one step further, if one calculates the dosimeter doses presented in Table IV using the calibration equations developed in Appendix C and corrects the measured dosimeter responses for the angle of incidence of the radiation on the dosimeter, the doses obtained are within four per cent of those calculated using $(R_s/R_{E_1}) = 1.0$ and this difference can be attributed to the regression analysis used in developing these two calibration equations.

It might further be argued that the fact that the doses obtained using the calibration equations developed in Section 5.0 converge to both the doses calculated using $(R_s/R_{E_1}) = 1.0$ and using the calibration equation of Appendix C is a necessary condition, but not sufficient to substantiate the validity of the calibration equations of Section 5.0. Although this argument is valid in that the doses obtained using these different calibration equations must

all converge to the same doses (including the collimator effects) it neglects one important factor. Since both calibration curves (that of Appendix C and those of Section 5.0) converge to the same doses when no correction is made for the collimator interactions then the only source of error left is in the ratio R_s/R_{E_1} or in the source strengths of the cobalt-60 sources used in obtaining the scattered gamma-ray distributions. Now the ratio R_s/R_{E_1} was determined using the curve of the collimator correction factor R versus the gamma-ray energy described in Section 5.0 and this curve is identical, within a few per cent, to the curve used in making corrections for the collimator interactions in the development of the response matrix. Hence a change in the curve of the collimator correction factor versus gamma-ray energy should result in an approximately equal change of magnitude in both the spectral and dosimeter doses.

With reference to the cobalt-60 source used in the dosimeter measurements it was found that the calibrated value of 82.6 ± 1.8 curies was within statistical agreement of the value quoted by the vendor. The strength of the cobalt-60 source used in the spectral measurements (0.243 ± 0.007 curies) was approximately twenty-two per cent lower than the vendor's quoted value. However upon calibrating this source again using a different experimental configuration and detector, a value for the source strength was determined which was within five per cent of the value obtained in the previous calibration. Thus it was concluded that the vendor's value for this source was in error and that the value (0.243 ± 0.007 curies) used in this report was correct.

There is one further point which must be considered concerning the applicability of the calibration curves of Section 5.0 to the dosimeter responses obtained from the scattered gamma-ray measurements. In particular,

consideration must be given to the difference in the angular distributions of the plane source used in developing the calibration curves and the simulated plane sources considered in the scattered gamma-ray measurements. Now the response of the dosimeter is proportional to the magnitude, as well as the spatial distribution, of the gamma-ray flux throughout the volume of the dosimeter and these quantities are in turn dependent on the angular distribution of the plane source. The magnitude of the gamma-ray flux incident on the detector is taken into account by the very nature of the calibration curves. However the calibration curves do not apply when the spatial distribution of the gamma-ray flux throughout the volume of the dosimeter is different from that encountered in the calibration experiment of Section 5.0. Now in the calibration experiment of Section 5.0 a plane isotropic source was used whereas in the scattered radiation measurements the angular distributions of the plane sources were anisotropic (17,18).

Now since it was previously stated that the spatial distribution of the gamma-ray flux was dependent on the angular distribution of the plane source a theoretical investigation of this problem was carried out. (See Appendix E.) This investigation was designed to determine if the differences in the angular distributions which were encountered in this work could result in a significant change in the spatial distribution of the gamma-ray flux throughout the volume of the dosimeter. Expressions were derived for the spatially dependent gamma-ray flux as a function of position in the collimator for various plane source angular distributions. The numerical results obtained from this investigation indicated that for the angular distribution of the scattered radiation sources simulated in this section the spatial distribution of the gamma-ray flux throughout the volume of the dosimeter was nearly

the same as that resulting from the isotropic source used in the dosimeter calibration experiment of Section 5.0. Therefore it was concluded that the difference in the angular distributions of the plane sources used in the calibration experiment of Section 5.0 and those encountered in this section did not have any effect on the applicability of the calibration curves of Section 5.0 to the dosimeter responses obtained in the scattered gamma-ray measurements of this section.

From the preceding discussion it appears that the method used to determine the dosimeter doses presented in Table IV was valid. In addition, it has been pointed out that the approximations used in developing the equations for the calibration curves of Section 5.0 could result in a total error, the magnitude of which could be as high as fifteen per cent. Therefore the maximum error associated with the dosimeter doses presented in Table IV has a range of from 17.9 to 18.0 per cent. Hence the previous discussion indicates that, within the maximum error limits presented above, the dosimeter doses tabulated in Table IV are accurate representations of the exposure doses resulting from the experimental configurations considered in this work.

With the establishment of the accuracy of the dosimeter doses as stated in the previous paragraph and since the spectral and dosimeter doses are still not within statistical agreement (their error limits do not overlap), then following the reasoning developed in Section 2.2, it must be concluded that there is an error in the spectral doses presented. As three different experimental configurations were considered and the geometry of each was reproduced three times it is not likely that such an error, which appears to be systematic, is due to the experimental spectral measurements. This indicates that the error is in the unfolding codes. Previously it was

pointed out (see page 42) that the appearance of negative values in the unfolded pulse-height distributions as illustrated in Figures 8, 9 and 10 indicated that the response matrix was not completely valid. Also a possible source of error which could result in systematic errors such as evidenced in this work is the incorrect normalization of the response functions used in generating the response matrix.

Since a detailed analysis of the unfolding codes is beyond the scope of this work no further comments can be made concerning the source of errors in the unfolding codes on the basis of this work. However, it should be noted that the development of new response functions and a new response matrix for the collimator spectrometer system used in this work are the subjects of two research projects (19,20) currently underway in the Department of Nuclear Engineering at Kansas State University.

7.0 CONCLUSIONS

As a result of this work the following conclusions can be made concerning the experimental method used in evaluating the unfolding technique.

- 1) The method used in calibrating the dosimeter for polyenergetic radiation using a calibrated plane source of cobalt-60 was valid.
- 2) The dosimeter doses obtained using the calibration referred to in 1) were accurate representations, within the maximum error limits, of the true exposure doses resulting from the experimental configurations considered.
- 3) The experiment designed was adequate to enable a determination of the accuracy of the exposure doses computed using the unfolding technique.

Also it was found that the spectral doses obtained using the unfolding codes considered in this work were larger than the dosimeter doses and were not within one standard deviation of the dosimeter doses. Therefore, since the results of this work indicated that the dosimeter doses were accurate, within their maximum error limits, it was concluded that the spectral doses were in error. This error appeared to be systematic. Furthermore it was concluded that the most probable source of this error was in the normalization of the response functions and/or the generation of the response matrix itself.

Although a detailed analysis of the unfolding codes was beyond the scope of this work the results of this work do indicate that such an analysis of the unfolding codes is warranted. At the present time work is progressing towards the development of new response functions and a new response matrix (19,20) which it is hoped will correct for the shortcomings of the response matrix considered in this work.

8.0 SUGGESTIONS FOR FURTHER STUDY

The primary purpose of this work was to develop a method for determining the accuracy of exposure doses calculated using an unfolding technique and the application of this method to a particular unfolding technique. An obvious extension of this work would be to develop an experiment to determine the accuracy of the unfolded pulse-height distributions. This could be accomplished using the collimator-spectrometer system to measure scattered radiation for selected gamma-ray scattering angles. The scattering angles chosen would necessarily be those for which Monte Carlo results are available. Then the unfolded pulse-height distributions could be compared against the Monte Carlo results.

The results of this work clearly indicated that the unfolding codes developed for the collimator-spectrometer system used in this work should be examined in detail. Towards this end, the development of new response functions and a new response matrix for this system is currently in progress (19, 20). The ability of the unfolding codes, using this new response matrix, to accurately predict exposure doses can be determined using the experimental spectra measured for this work and comparing the resulting spectral doses to the dosimeter doses in the manner outlined in this report.

The dependence of the collimator correction factor on the gamma-ray energy also deserves further experimental work. As was previously noted, Mather has investigated this problem in detail on a theoretical basis; however, there is a scarcity of experimental results in the literature on this subject. The relationship between the collimator correction factor and the gamma-ray energy could be investigated using the techniques presented in this work. This would involve using the plane simulator with a number of monoenergetic sources having a range of gamma-ray energies.

Also this work has indicated that there is a need for more experimental work on the angular-energy dependence of the Victoreen ten milliroentgen dosimeter. An experimental study of this nature would be especially valuable at low gamma-ray energies. However, at these low energies one of the greatest obstacles is the acquisition of appropriate monoenergetic sources.

9.0 ACKNOWLEDGEMENT

The author wishes to express his sincere appreciation to Dr. R. E. Faw under whose guidance this work was accomplished. Thanks are extended to Mr. J. A. Baran and Mr. R. M. Rubin for their help and advice concerning the unfolding codes and the experimental phase of this work. Also, appreciation is extended to Dr. W. R. Kimel, Head of the Department of Nuclear Engineering at Kansas State University, for his support and encouragement during the course of this work. To Miss S. J. Wilson is extended a special word of thanks for her diligence in typing this report.

10.0 LITERATURE CITED

1. Childers, H. M.
Analysis of Single Crystal Pulse-Height Distributions, Review of Scientific Instruments, 30 (September, 1959) No. 9, pp. 810-814.
2. Heath, R. L.
Analysis of Complex Gamma Spectra, NYO 10595, Proceedings of the Conference on the Utilization of Multiparameter Analyzers in Nuclear Physics held by Columbia University at Grossinger, New York, Nov. 12-15, 1962, pp. 120-131.
3. Heath, R. L.
Data Analysis Techniques for Gamma-ray Scintillation Spectrometry, IDO-16784, AEC Research and Development Report, TID-4500 (17th ed.) May 29, 1962.
4. Hubbell, J. H.
Response of a Large Sodium-Iodide Detector to High-Energy X-Rays, The Review of Scientific Instruments, 29 (January, 1958) No. 1, pp. 65-68.
5. Hydo, Tomonori and Makino, Fumiyoshi
Response Function of a Three-inch Diameter by Three-inch Long NaI(Tl) Scintillator to Gamma-Rays, Reprint from Memoirs of the Faculty of Engineering, Kyoto University, Kyoto, Japan, Vol. XXIV (April, 1962) Part 2.
6. Mollenauer, James F.
A Computer Analysis for Complex Sodium Iodide Gamma Spectra, UCRL-9748, Lawrence Radiation Laboratory, Berkeley, California, UC-34 Physics, TID-4500 (16th ed.) August, 1961.
7. Scofield, N. E.
A Technique for Unfolding Gamma-Ray Scintillation Spectrometer Pulse-Height Distributions, USNRDL-TR-447, June 24, 1960.
8. Scofield, N. E.
Iterative Unfolding, Applications of Computers to Nuclear and Radio-chemistry, Proceedings of a Symposium, Gatlinburg, Tennessee, October 17-19, 1962, NAS-NS 3107.
9. Trombka, J. I.
Least Squares Analysis of Gamma-Ray Pulse Height Spectra, NASA, Technical Report 32-373, Jet Propulsion Laboratory, California Institute of Technology, Pasadena, California, December 15, 1962.
10. Kimel, W. R., Faw, R. E., Baran, J. A., et al.
Scattering of Fallout Radiation from Ceilings of Protective Structures, Special Report Number 72, Kansas Engineering Experiment Station, Manhattan, Kansas, July, 1966.

11. Technical Operations Incorporated
Operation Manual for Model 402 Gamma Ray Projector
12. Technical Operations Incorporated
Operation of Tech/Ops Model 539 Duplex Hydraulic Source Circulation System, Manual No. TO-B 62-38, June 15, 1962, Burlington, Massachusetts.
13. Mather, R. L.
Gamma-Ray Collimator Penetration and Scattering Effects, Journal of Applied Physics, 28 (October, 1957) No. 10, pp. 1200-1207.
14. Tomnovec, F. M. and Mather, R. L.
Experimental Gamma-Ray Collimator Sensitivity Patterns, Journal of Applied Physics, 28 (October, 1957) No. 10, pp. 1208-1211.
15. Burson, Z. G., Summers, R. L. and Brashears, J. T.
Mobile Radiological Measuring Unit: Description and Operating Information, Edgerton, Germeshauser and Grier, Inc., CEX-63.11 (February, 1965).
16. Baran, J. A.
Personal Communication, Department of Nuclear Engineering, Kansas State University, Manhattan, Kansas.
17. Huddleston, C. M. and Shoemaker, N. F.
A Mathematical Derivation of Contour Lines for Constant Albedo of Gamma Rays on Concrete, TN-539, DASA 11.026, U. S. Naval Civil Engineering Laboratory, Port Hueneme, California, Oct. 31, 1963.
18. Huddleston, C. M.
Private Communication to J. A. Baran, Physics and Mathematics Division, U. S. Naval Civil Engineering Laboratory, Port Hueneme, Calif., Aug. 10, 1965.
19. Reynolds, R.
Master of Science Thesis, Department of Nuclear Engineering, Kansas State University, Manhattan, Kansas, to be published.
20. Baran, J. A.
Ph.D. Dissertation, Department of Nuclear Engineering, Kansas State University, Manhattan, Kansas, to be published.
21. Fite, L. E., Gibbons, D. and Wainerdi, R. E.
A System for the Control of Drift in a Multi-channel Gamma Ray Spectrometer, Proceedings of the 1961 International Conference on Modern Trends in Activation Analysis, Texas A&M College, College Station, Texas, December 15-16, 1961.
22. de Waard, H.
Stablizing Scintillation Spectrometers with Counting Rate Differences Feedback, Nucleonics, 13 (July, 1955) pp. 36-41.
23. Covell, D. F.
Quality Control for the Gamma-Ray Scintillation Spectrometer, USNRDL-TR-584, September, 1962.

24. Crouch, D. F. and Heath, R. L.
Routine Testing and Calibration Procedures for Multichannel Pulse Analyzers and Gamma-Ray Spectrometers, IDO-16923, Phillips Petroleum Co., A. E. Division, November 1, 1963.
25. Technical Measurements Corporation
Instruction Manual, Models 402 and 404, 400 Channel Pulse-Height Analyzer, Vol. I, North Haven, Connecticut, 1962.
26. Clark, E. T. and Batter, J. F.
Gamma Ray Scattering by Concrete Surfaces, Nuclear Science and Engineering, 17 (September, 1963) No. 1, pp. 125-130.
27. Chilton, A. B., Holoviak, D. and Donovan, L. K.
Determination of Parameters in an Empirical Function for Build-up Factors for Various Photon Energies, U. S. Civil Engineering Laboratory, Technical Note, N-389, August, 1960.
28. Hine, Gerald J. and Brownell, Gordon L. (editors)
Radiation Chemistry, Academic Press, Inc., New York, 1956.
29. Grotenhuis, M.
Lecture Notes on Reactor Shielding, ANL-6000, Argonne National Laboratory, Lemont, Illinois, March, 1959.
30. Mandel, J.
The Statistical Analysis of Experimental Data, Interscience Publishers, New York, New York, 1964.
31. Brownlee, K. A.
Statistical Theory and Methodology in Science and Engineering, John Wiley and Sons, Inc., New York, New York, 1965.

11.0 APPENDICES

APPENDIX A

SPECTROMETER QUALITY CONTROL

In order that some degree of confidence could be placed on the spectral data obtained using the gamma-ray scintillation collimator-spectrometer system, a quality control program was initiated to be used with this system. Although quality control is primarily concerned with maintaining the quality of a system at a certain level and not the establishment of quality, it is apparent that through the correction of deficiencies in the system the quality of the system as a whole may be improved.

The quality control of scintillation spectrometers has been extensively investigated (21,22,23,24) and the results have indicated that drifts in the gain and baseline may completely invalidate the calibration of the system and in any case will decrease the precision of any measurements which might be made. These drifts result in fluctuations in the energy per channel and the total energy range being examined through the use of the multichannel analyzer.

It is of prime importance to maintain a constant value for the energy per channel and the total energy range when employing a scintillation spectrometer system. However, drift in the baseline (zero energy position) and/or the overall gain of the system will change these values. Drift due to fluctuations in the gain is primarily attributed to small changes in (1) the conversion and optical efficiency of the crystal, (2) the photomultiplier tube gain, and (3) the linear amplifier gain. Gain drift results in a change of the energy per channel of the system. The zero energy intercept or baseline is determined by the acceptance threshold of the multichannel

analyzer. Hence a baseline drift will uniformly shift the entire spectrum as well as relocate the position of the zero energy channel.

Fite et al. (21) have developed a system to correct for the drift due to gain changes and changes in the baseline or zero point of the analyzer system. Their method utilizes two radioactive sources as standards and the multichannel analyzer core memory is then monitored to determine if the peaks are in the proper channels. If the peaks do not appear in the proper channels the gain and/or baseline are altered through the use of a servo-system to bring the peaks to the correct channels.

A similar system has been developed by de Waard (22) to correct for drifts due to fluctuations in the gain. However, he considers only the drift in gain and indicates that perturbations in the system due to baseline drift are negligible compared to those caused by drift in the gain. Corrections for the drift in gain are made through the use of a feedback system to the photomultiplier tube voltage.

Covell (23) has pointed out that the above techniques introduce extraneous "background" spectra which tend to complicate the interpretation of the measured spectrum. Therefore, for this research, a control procedure was developed which utilized a daily check of the analyzer system using a zinc-65 source as a standard. Corrections were then made manually to compensate for any changes in the gain and baseline demonstrated by the spectrum for the standard source. A similar program for quality control has been incorporated by Crouch and Heath (24) in their work. Although these two methods (23,24) of obtaining a control over the analyzer system do not provide a continuous monitor of the system they do eliminate the extraneous "background" spectrum noted earlier.

In order for the quality control program initiated for this work to be effective it was necessary that the entire procedure (daily sampling, data evaluation, logging and estimation of the quality) be as brief as possible and still maintain a high level of efficiency.

This quality control program is in agreement with Covell (23) and Crouch and Heath (24) insofar as drift in the baseline is considered to be an important contributor to the overall drift in the system as a whole. Therefore the daily check on the quality of the system included a means of correcting the drift due to both effects.

The standardization of the spectrometer system was repeated as often as was deemed necessary but at least once daily. The pulse height and position of each photopeak was determined from the spectrum obtained. The positions of these photopeaks were compared with the preset location for each peak. If drift in the system had occurred, the gain and/or baseline of the multichannel analyzer were altered manually to return the peaks to the proper channels.

The zinc-65 source was chosen as the standard since it emits two readily detected and well separated gamma rays (0.51 and 1.114 MeV) in the energy region of interest and because it has a sufficiently long half-life (245 days). Although this is a short half-life compared to standard sources in general, it was long enough to render the problem of source decay negligible over the period of its use. The strength of the source and its position relative to the detector were selected such that there would be no drift induced because of an excessively high count rate. Care was taken in positioning the source in order that a constant geometry between the source and the scintillation detector might be maintained from day to day.

In addition to the daily monitor on the gain and baseline, a routine examination was made daily to determine if the multichannel analyzer were operating correctly. This examination consisted of several tests designed to evaluate whether the memory location and computer sections of the analyzer were performing properly and was carried out in the manner outlined in the manufacturer's operating manual (25).

To avoid small drifts in the system resulting from changes in the temperature of the scintillation detector the scintillation crystal and photomultiplier tube were kept at approximately 106°F by employing a constant temperature circulating water pump to force heated water through coils located within the collimator (Figure 2). Because of the large mass of the collimator (approximately 3500 pounds), a period of about twenty-four hours was required to raise the temperature of the collimator to the desired level. After the temperature had stabilized, the thermostatically-controlled pump was operated continuously to maintain the temperature of the system. Although the face of the crystal was exposed to the ambient temperature through the two-inch by fourteen-inch collimator, this system did minimize both the chance of a sudden change in the temperature of the crystal-photomultiplier tube assembly, and the spectral drift which would accompany such a temperature change.

The multichannel analyzer and associated instruments were kept in a closed, air conditioned room. This was done to decrease the possibility either of the instruments overheating or of failure of the readout equipment because of dirt in the mechanical parts.

The quality control program proved to be of great aid in maintaining good quality control for the gamma-ray scintillation spectrometer system as

compared to the system performance previous to the initiation of this program. Because of the nature of the experimental measurements made with this system it was extremely difficult to determine if the system was operating properly without first analyzing the experimental data obtained. Therefore this quality control program was particularly valuable in that it provided an early indication of system deficiencies and their probable location in the system, thereby saving experimental time which would have otherwise resulted in the acquisition of highly erratic experimental data.

APPENDIX B

CALIBRATION OF THE COBALT-60
SIMULATED PLANE ISOTROPIC SOURCE

The plane isotropic source of cobalt-60 which was simulated using the line source and the plane simulator illustrated in Figures 3 and 4 was calibrated in the configuration of Figure 11 using the Victoreen ten-milliroentgen full-scale dosimeter which had been calibrated in the manner described in Appendix C. Measurements were made for one complete simulation of the plane source and two source-to-detector distances. A minimum of three measurements were made for each of the two distances. From an investigation of the background for a time equivalent to that required for a simulation of the source plane, it was concluded that the dose due to background was negligible. The dosimeter was read using the Technical Operations charger-reader and these readings in microamperes were then corrected for temperature and pressure using Eq. (C-1) of Appendix C. The readings were then normalized to an exposure time of twenty-eight minutes.

The experimental dosimeter responses in microamperes were averaged for each plane source-to-detector distance and converted to doses in milliroentgens using Eq. (C-19) of Appendix C. Experimental dosimeter responses in microamperes, corrected for temperature, pressure and exposure time, and the corresponding doses in milliroentgens for each of the two cases considered, are presented in Table B-1.

Using the doses from Table B-1, the strength of the plane source D_p^* in milliroentgens per twenty-eight minutes was determined from

*Although D_p , which could not be measured experimentally, has the units of dose, it actually represents the product of source strength, exposure time and the flux to dose conversion factor. This unusual term was employed for convenience in carrying out the calculations.

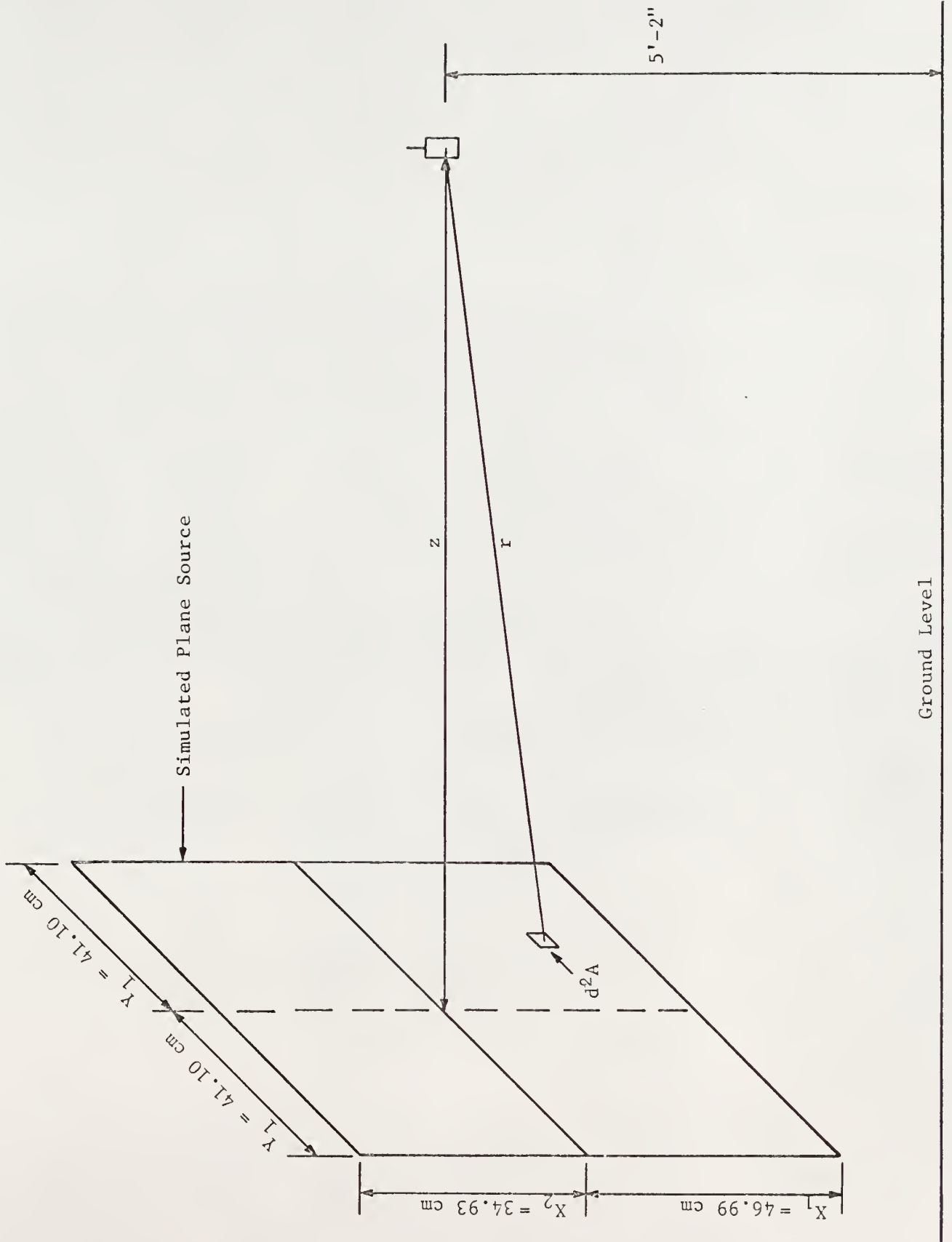


Figure 11. Experimental configuration for plane source calibration

Ground Level

$$D_z = \iint_{\text{Area of plane source}} \frac{D_P}{4\pi r^2} d^2A \quad (\text{B-1})$$

in which D_z = dose in mr for the detector at a distance z from the plane source,

d^2A = differential area on the plane source, and

r = distance from d^2A to the detector position in centimeters.

Table B-1. Experimental dosimeter responses and their corresponding average doses used in the calibration of the simulated plane source.

Plane Source-to-Detector Distance (feet)	Dosimeter Response Normalized to 28 Minutes (microamperes)	Average Dose Normalized to 28 Minutes (milliroentgens)
12.0	25.50 27.12 25.70 25.91	2.71 ± 0.09
14.0	19.35 19.58 19.57	2.02 ± 0.07

Assuming that the plane source is uniform and referring to Figure 11, the preceding equation becomes

$$D_z = \frac{D_P}{4\pi} \int_0^{Y_1} dy \left[\int_0^{X_1} dx \frac{2}{(x^2+y^2+z^2)} + \int_0^{X_2} dx \frac{2}{(x^2+y^2+z^2)} \right] \quad (\text{B-2})$$

Integration with respect to x yields

$$D_z = \frac{D_p}{4\pi} \int_0^{Y_1} dy \frac{2}{(y^2+z^2)^{1/2}} \left[\tan^{-1} \frac{X_1}{(y^2+z^2)^{1/2}} + \tan^{-1} \frac{X_2}{(y^2+z^2)^{1/2}} \right] \quad (B-3)$$

and solving for D_p results in

$$D_p = 4\pi D_z \div \left\{ \int_0^{Y_1} dy \frac{2}{(y^2+z^2)^{1/2}} \left[\tan^{-1} \frac{X_1}{(y^2+z^2)^{1/2}} + \tan^{-1} \frac{X_2}{(y^2+z^2)^{1/2}} \right] \right\}. \quad (B-4)$$

The integral term in the denominator of Eq. (B-4) was evaluated for the two values of plane source-to-detector distance using a Gaussian quadrature technique. The numerical integration was programmed for the IBM-1410 digital computer. Substitution of the appropriate values into Eq. (B-4) for each plane source-to-detector distance resulted in a value of D_p for each of the two cases.

It should be noted that Eq. (B-4) does not take into account the effects of the exponential attenuation in air or the buildup factors due to air and ground scattering. Since the product of these three terms could be considered as a constant value over the area of the plane source, an average value for this product was determined (26,27) for each of the plane source-to-detector distances. The values used were 1.053 and 1.039. These numbers correspond to source-to-detector distances of fourteen and twelve feet respectively. Thus the values of D_p obtained from Eq. (B-4) were divided by the appropriate value (1.053 or 1.039) to correct for exponential attenuation and buildup due to scattering. These two values were then averaged to yield

$$D_p = 657 \pm 16 \text{ milliroentgens.} \quad (\text{B-5})$$

This value of D_p is proportional to the source strength for the simulated plane isotropic source of cobalt-60.

APPENDIX C

CALIBRATION OF THE DOSIMETER
USING A POINT SOURCE

A calibration curve was developed to determine the relationship between the dosimeter response, i.e., the microampere reading obtained with the Technical Operations charger-reader, and the exposure dose in milliroentgens when the dosimeter was exposed to a point source. This was accomplished by computing a regression line using the experimentally measured dosimeter responses and theoretically calculated exposure dose.

The experimental data were obtained by exposing the dosimeter to a calibrated point source of cobalt-60 for various time increments. A calibration board, constructed in such a manner as to minimize gamma-ray scattering, was utilized so that the source-to-detector distance could be maintained at a constant value. This calibration board was suspended above ground level in order to decrease ground scattering. This experimental configuration is illustrated in Figure 12.

The data were corrected to a temperature and pressure of 22°C and 760 mm of mercury by multiplying the experimental dosimeter response in microamperes by a dimensionless correction factor defined by

$$\alpha = \frac{[273.0 + 0.555 (T-32.0)] 760.0}{(295.0) (25.40) P} \quad (C-1)$$

in which T was the temperature in degrees Fahrenheit and P was the pressure in inches of mercury during the experimental run.

The exposure dose rate which would be expected from the experiment can be theoretically computed using

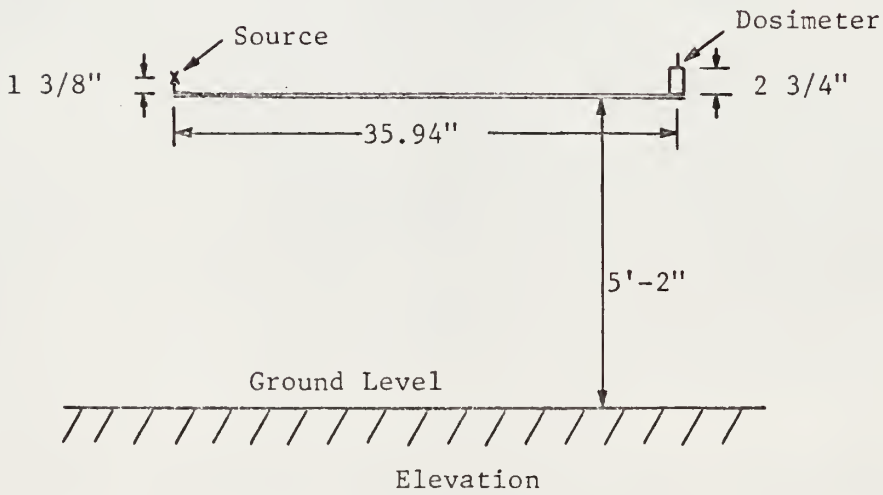
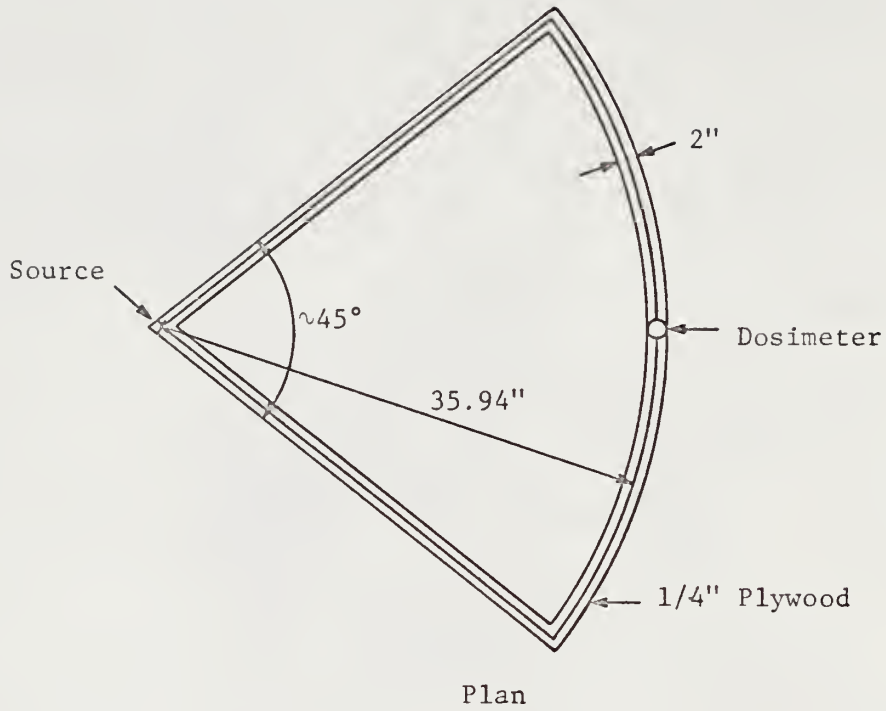


Figure 12. Experimental configuration for the dosimeter calibration using a point source

$$D_{Th}^{E_1} \left(\frac{mr}{hr} \right) = \frac{K S B_1 B_2 e^{-\mu x}}{4\pi x^2} \quad (C-2)$$

in which $D_{Th}^{E_1} \left(\frac{mr}{hr} \right)$ = theoretical exposure dose rate in milliroentgens per hour,

K = conversion factor (mr/hr)/(mc/cm²),*

S = strength of the cobalt-60 source in millicuries,

B_1 = buildup factor for air scattering

B_2 = buildup factor for ground scattering,

μ = total gamma-ray attenuation coefficient (cm⁻¹) for 1.25 MeV gamma rays, and

x = source-to-detector distance in centimeters.

The strength of the source on the date of the experiment is calculated using

$$S = S_i \exp(-0.693 t/t_{1/2}) \quad (C-3)$$

in which S_i = strength of the cobalt-60 source in millicuries on the date of its calibration,

t = time in years between the date corresponding to S_i and that corresponding to S , and

$t_{1/2}$ = half-life of cobalt-60 in years.

Substitution of the appropriate values into Eq. (C-3) yields

$$S = (6.67 \text{ mc}) \exp((-0.693/5.27)4.06) = 3.91 \text{ mc} \quad (C-4)$$

where $S_i = 6.67 \text{ mc}$ on October 31, 1961.

*The units for this conversion factor (mr/hr)/(7.4x10⁷ photons/cm²-sec) have been chosen to facilitate evaluation of Eq. (C-2) with S expressed in millicuries.

The conversion factor K was based on the definition of the roentgen. One roentgen corresponds to the dose given to one gram of air when 83.8 ergs of energy are absorbed in that mass of air (28). Then the energy flux per roentgen is defined by

$$\phi_E = \frac{83.8 \text{ ergs}}{\left(\frac{\mu_a}{\rho}\right)_{\text{air}} r\text{-cm}^2} \quad (\text{C-5})$$

in which $(\mu_a/\rho)_{\text{air}}$ is the gamma-ray energy absorption mass attenuation coefficient. Converting from ergs to MeV yields

$$\phi_E = \frac{5.23 \times 10^7 \text{ MeV}}{\left(\frac{\mu_a}{\rho}\right)_{\text{air}} r\text{-cm}^2} \quad (\text{C-6})$$

Now let $\phi_E = 1.0$ and then Eq. (C-6) can be written as

$$1.0 \text{ r} = \frac{5.23 \times 10^7 \text{ MeV}}{\left(\frac{\mu_a}{\rho}\right)_{\text{air}} \text{cm}^2} \quad (\text{C-7})$$

From Grotenhuis (29), the value of $(\mu_a/\rho)_{\text{air}}$ for 1.25 MeV gamma rays (this is the average energy of the two gamma rays emitted by cobalt-60) is 0.268 cm^2/gm . Substituting this value into Eq. (C-7) and converting from MeV to curie-second yields

$$\begin{aligned} 1.0 \text{ r} &= \left[\frac{5.23 \times 10^7 \text{ MeV}}{0.268 \text{ cm}^2} \right] \left[\frac{1 \text{ } \gamma}{1.25 \text{ MeV}} \right] \left[\frac{1 \text{ disintegration}}{2 \text{ } \gamma} \right] \left[\frac{1 \text{ curie}}{3.7 \times 10^{10} \text{ dis}} \frac{\text{dis}}{\text{sec}} \right] \\ &= 2.11 \times 10^{-2} \frac{\text{curie-sec}}{\text{cm}^2} \end{aligned} \quad (\text{C-8})$$

$$\text{or } 1 \text{ r} = 0.586 \times 10^{-5} \frac{\text{curie-hr}}{\text{cm}^2} \quad (\text{C-9})$$

Thus the conversion factor K is

$$K = 1.71 \times 10^5 \text{ (mr/hr)/(mc/cm}^2\text{)} . \quad (\text{C-10})$$

The source and detector were suspended five feet two inches above ground level and 91.3 cm apart as shown in Figure 12. With these parameters and using the experimental curve presented by Clark and Batter (26), the buildup factor for ground scattering, B_2 , was found to be 1.00686.

The value of the buildup factor due to air scattering was obtained from the expression (27)

$$B_1 = 1.0 + 0.92 \mu x e^{0.0632 \mu x} . \quad (\text{C-11})$$

in which μx is the source-to-detector distance in mean free paths of air. Substitution of the appropriate value of μx yields $B_1 = 1.00552$. The value for the exponential attenuation was

$$e^{-\mu x} = 0.994 . \quad (\text{C-12})$$

The substitution of the appropriate values into Eq. (C-2) results in a theoretical exposure dose rate of

$$D_{\text{Th}} \left(\frac{\text{mr}}{\text{hr}} \right) = \frac{(1.71 \times 10^5)(3.91)(1.00552)(1.00686)(0.994)}{4\pi(91.3)^2} = 6.41 \frac{\text{mr}}{\text{hr}} . \quad (\text{C-13})$$

The experimental dosimeter responses and the theoretical doses are presented in Table C-1. The experimental dosimeter responses listed in this table have been corrected for temperature and pressure according to Eq. (C-1).

It is imperative at this point to have a basic understanding of the dosimeter and the charger-reader if a curve is to be fitted to the data presented in Table C-1. In the use of this detection system the dosimeter is

Table C-1. Data used in the calibration of the dosimeter using a point source

Exposure Time (minutes)	Dosimeter Response (microamperes)	Theoretical Dose (milliroentgens)
15.0	15.53	1.60
	15.53	
	16.05	
25.0	25.84	2.67
	25.27	
	26.31	
	25.81	
35.0	36.16	3.74
	35.65	
	35.62	

initially charged to a given voltage corresponding to a zero reading on the charger-reader meter scale. When the dosimeter is exposed to ionizing radiation electrons are ejected from the dosimeter walls which in turn result in the production of ion pairs in the dosimeter chamber gas. These ion pairs are then swept away to the detector electrodes due to the potential gradient across the dosimeter. Upon reaching the electrodes, the ion pairs have the effect of neutralizing a portion of the original dosimeter charge. When the dosimeter is read using the charger-reader the output voltage is the difference between the dosimeter voltage and the original charging voltage. This output voltage is thus a linear function of the charge collected, i.e., the integrated dose received by the dosimeter.

In the interest of clarity and with the preceding discussion in mind, a word of explanation is in order concerning the units on the charger-reader

meter scale. The units of this scale and thus the units associated with the dosimeter responses presented in this report are microamperes. However, in the preceding paragraph it was stated that the quantity measured was a voltage. Thus there appears to be a contradiction between the quantity measured and the quantity which is obtained from the charger-reader meter scale. This apparent contradiction results from the fact that when the manufacturer assembled the charger-reader an ammeter was modified in order to make it voltage rather than charge sensitive but the appropriate change was not made in the units on the scale of this meter. However, because the dosimeter and charger-reader must be calibrated before being used and because the needle deflection on the charger-reader meter scale is a linear function of the dose received by the dosimeter the units given on this scale are not really significant. Thus in order to avoid confusing the reader who is familiar with this particular charger-reader the author has elected to report the dosimeter response in terms of the units given on the meter scale, i.e., microamperes.

From the preceding discussion concerning the linearity between the deflection of the needle on the charger-reader meter scale and the integrated exposure dose received by the dosimeter, then if the charger-reader meter is zeroed preceding the charging of the dosimeter, a zero exposure of the dosimeter to ionizing radiation should result in a zero microampere reading on the charger-reader. Following a check of the charger-reader and dosimeter it was observed that for no exposure to radiation the dosimeter response was indeed zero. Also upon investigation, it was learned that the drift, i.e., loss of initial charge due to leakage and other effects, in the dosimeter charge was less than 0.5 microamperes per hour. Thus it was concluded that loss of charge because of drift was negligible.

Therefore with the knowledge that the response of the dosimeter to ionizing radiation is a linear function of the integrated dose to which the dosimeter was exposed and that for no exposure to radiation the dosimeter response is zero, the data of Table C-1 were fitted to a straight line passing through the origin using the regression analysis outlined in Appendix D. The experimental dosimeter responses were taken as the y values and the theoretical doses as the x values in this analysis. The values of x had a constant percentage error equivalent to that associated with the calibration source strength. Thus the Berkson model (30) for a controlled experiment was utilized. (See Appendix D.) From Eq. (D-6) of Appendix D the slope of the line is

$$b = \frac{\sum_{i=1}^{10} x_i y_i}{\sum_{i=1}^{10} (x_i)^2} = 9.63 . \quad (\text{C-14})$$

The estimate of the variance, σ^2 , from Eq. (D-20) of Appendix D is

$$(s')^2 = s^2 + b^2 V[x] \quad (\text{C-15})$$

in which

$$s^2 = \frac{\sum_{i=1}^{10} (y_i)^2 - \frac{(\sum_{i=1}^{10} x_i y_i)^2}{10}}{\sum_{i=1}^{10} (x_i)^2} = 0.148 \quad (\text{C-16})$$

and

$$b^2 V[x] = b^2 \left[0.05 \left(\frac{\bar{y}'}{b} \right) \right]^2 = (0.05 \bar{y}')^2 \quad (\text{C-17})$$

where \bar{y}' is the mean of m new observations and the 0.05 represents the standard deviation in the calibration source strength.

Since the calibration curve was to be used to convert from microamperes to milliroentgens, the least squares line in reverse was determined. To calculate the value of x corresponding to some \bar{y}' , the equation

$$x = \frac{\bar{y}'}{b} \pm \frac{ts'}{b} \left[\frac{1}{m} + \frac{(\bar{y}')^2}{b^2 \sum_{i=1}^{10} (x_i)^2} \right]^{1/2} \quad (C-18)$$

can be used if the condition on g' , as defined by Eq. (D-22) of Appendix D, is satisfied. The value of t is 1.05 for 68% confidence (one standard deviation) and nine degrees of freedom. The value of g' in the range of interest is much less than 0.1 and thus the least squares line in reverse, as given above, is valid. Substitution of the values of b, s', t and $\sum_{i=1}^{10} (x_i)^2$ as calculated from the data given in Table C-1 yields

$$x = 0.104 \bar{y}' \pm 0.109 [0.148 + (0.05 \bar{y}')^2]^{1/2} \left[\frac{1}{m} + 0.000138 (\bar{y}')^2 \right]^{1/2}. \quad (C-19)$$

APPENDIX D

REGRESSION ANALYSIS

The method of least squares is a mathematical technique for fitting an "optimum" curve through a given number of points. This optimum curve is obtained by determining the parameters of the curve in such a way as to minimize the sum of the squares of the deviations between the values of the observed and predicted points. In fitting a straight line which passes through the origin to a set of data points, the following two cases must be considered: 1) one variable subject to error and the other with negligible error and 2) both variables subject to error.

Following the method outlined by Brownlee (31), the case where y is observed with error and x is assumed to be free of error is considered first. In addition, it is assumed that the observed values of y have a normal distribution about the expected value γ with a variance σ^2 and that all observations are independent.

If the true equation of the line is represented by

$$\gamma = \beta x \quad (D-1)$$

then the least squares analysis of the data will yield estimates b and s^2 of β and σ^2 . Also this analysis will provide a method of determining the distribution of these estimates. Assume that, for each value of x_i , $i=1, 2, \dots, k$, there are n_i values of y_i . The data points can be considered by pairing each value of y_i with its corresponding value of x_i . For example, if $k=2$, $n_1=2$, and $n_2=3$, then the points

$$(y_{11}, x_1)(y_{12}, x_1)(y_{21}, x_2)(y_{22}, x_2)(y_{23}, x_2) \quad (D-2)$$

can be represented as

$$(y_1, x_1) (y_2, x_2) (y_3, x_3) (y_4, x_4) (y_5, x_5) , \quad (D-3)$$

where $x_1 = x_2$ and $x_3 = x_4 = x_5$.

Now if the estimated least squares line is represented by

$$Y = bx ,$$

then the sum of the squares of the deviations between the observed values y_i and the estimated values Y_i is

$$Q = \sum_{i=1}^{\ell} (y_i - Y_i)^2 = \sum_{i=1}^{\ell} (y_i - bx_i)^2 \quad (D-4)$$

in which ℓ is the total number of observations. The minimum of Q is obtained by taking the first derivative of Q with respect to b and equating it to zero,

$$\text{i.e.,} \quad \frac{dQ}{db} = -2 \sum_{i=1}^{\ell} (y_i - bx_i)x_i = 0, \quad (D-5)$$

$$\text{from which} \quad b = \frac{\sum_{i=1}^{\ell} x_i y_i}{\sum_{i=1}^{\ell} (x_i)^2} . \quad (D-6)$$

The estimate of σ^2 is defined as

$$s^2 = \frac{\sum_{i=1}^{\ell} (y_i - Y_i)^2}{(\ell - 1)} , \quad (D-7)$$

where $\ell - 1$ represents the degrees of freedom. Now

$$y_i = (y_i - Y_i) + Y_i = (y_i - Y_i) + bx_i . \quad (D-8)$$

Squaring this equation and summing over i yields

$$\sum_{i=1}^{\ell} (y_i)^2 = \sum_{i=1}^{\ell} (y_i - Y_i)^2 + \frac{(\sum_{i=1}^{\ell} x_i y_i)^2}{\sum_{i=1}^{\ell} (x_i)^2} . \quad (\text{D-9})$$

Thus

$$s^2 = \frac{\sum_{i=1}^{\ell} (y_i)^2 - [(\sum_{i=1}^{\ell} x_i y_i)^2 / \sum_{i=1}^{\ell} (x_i)^2]}{\ell - 1} . \quad (\text{D-10})$$

The least squares line can be used in reverse to calculate a value of x corresponding to some \bar{y}' , the mean of m new observations. The point estimate of x is obtained from

$$x = \frac{\bar{y}'}{b} . \quad (\text{D-11})$$

The value of \bar{y}' which would correspond to this value of x , using the true least squares line, is η .

From Eq. (D-1), the value of x corresponding to this value of η is

$$x = \frac{\eta}{\beta} \quad (\text{D-12})$$

and if this true value of x is designated by α , then

$$\eta - \alpha\beta = 0 . \quad (\text{D-13})$$

Define the variable w as

$$w \equiv \bar{y}' - b\alpha . \quad (\text{D-14})$$

The expected value of w can be represented by

$$E[w] = \eta - \alpha E[b] = \eta - \alpha\beta = 0 \quad (\text{D-15})$$

and its variance as

$$V[w] = V[\bar{y}'] + \alpha^2 V[b] = \frac{\sigma^2}{m} + \frac{\alpha^2 \sigma^2}{\sum_{i=1}^{\ell} (x_i)^2} . \quad (D-16)$$

Using the estimate of σ^2 given by Eq. (D-10), the value of x corresponding to \bar{y}' is

$$x = \frac{\bar{y}'}{b^2 - \frac{t^2 s^2}{\sum_{i=1}^{\ell} (x_i)^2}} \pm \frac{ts}{b^2 - \frac{t^2 s^2}{\sum_{i=1}^{\ell} (x_i)^2}} \left[\left[b^2 - \frac{t^2 s^2}{\sum_{i=1}^{\ell} (x_i)^2} \right] \frac{1}{m} + \frac{(\bar{y}')^2}{\sum_{i=1}^{\ell} (x_i)^2} \right]^{1/2} \quad (D-17)$$

where t is the fractional point of the t distribution based on $(\ell-1)$ degrees of freedom. The preceding equation for x is governed by a term g which is defined as

$$g = \frac{t^2 s^2}{b^2 \sum_{i=1}^{\ell} (x_i)^2} . \quad (D-18)$$

If the value of g is less than 0.1, then the approximation

$$b^2 - \frac{t^2 s^2}{\sum_{i=1}^{\ell} (x_i)^2} = b^2 \left[1 - \frac{t^2 s^2}{b^2 \sum_{i=1}^{\ell} (x_i)^2} \right] = b^2 (1-g) \approx b^2$$

can be used in Eq. (D-17). Thus, for the case where g is less than 0.1, the value of x corresponding to \bar{y}' can be determined from

$$x = \frac{\bar{y}'}{b} \pm \frac{ts}{b} \left[\frac{1}{m} + \frac{(\bar{y}')^2}{b^2 \sum_{i=1}^{\ell} (x_i)^2} \right]^{1/2} . \quad (D-19)$$

The case where both variables are subject to error can be treated by using the Berkson model for controlled experiments (30,31). Berkson noted that when an experiment was carried out in such a manner that the x variable was a "controlled" quantity (i.e., for each observation of y_i , the corresponding value of x was assigned a value x_i , which was as close to the true value of x_i as was experimentally possible), then the least squares line could be determined in the same manner as was previously described (one variable subject to error). However, for this case, the variance associated with the least squares line must contain a term which takes into account the error associated with the x variable.

For a least squares line through the origin, the slope of the line can be found using Eq. (D-6). The estimate of σ^2 is represented by Mandel as

$$(s')^2 = s^2 + b^2V[x] \quad (D-20)$$

where s^2 is defined by Eq. (D-10) and $V[x]$ is the variance associated with the "controlled" variable x.

In order to use the least squares line in reverse to find a value of x corresponding to the mean of m new observations, \bar{y}' , Eq. (D-17) should be used. However, the value of s in Eq. (D-17) must be replaced by the s' in Eq. (D-20). The expression for x is then

$$x = \frac{\bar{y}'}{b} \pm \frac{ts'}{b} \left[\frac{1}{m} + \frac{(\bar{y}')^2}{b^2 \sum_{i=1}^l (x_i)^2} \right]^{1/2} \quad (D-21)$$

under the condition that g' is less than 0.1. The value of g' is determined from

$$g' = \frac{t^2(s')^2}{b^2 \sum_{i=1}^l (x_i)^2} \quad (D-22)$$

APPENDIX E

UNCOLLIDED GAMMA-RAY FLUX IN THE COLLIMATOR
RESULTING FROM VARIOUS PLANE SOURCE ANGULAR DISTRIBUTIONS

This appendix is devoted to a theoretical investigation of the variation in the uncollided gamma-ray flux within a collimator resulting from changes in the angular distribution of a plane source located at one end of the collimator. In particular this study was intended to determine if the spatial distribution of the flux throughout the collimator varied as the angular distribution of the plane source was changed, and if so, the extent of this variation. The derivation of formulae for the uncollided flux as a function of position within the collimator was carried out using a general collimator-plane source geometry. This collimator-plane source geometry is illustrated in Figure 13 and consists of a right circular cylindrical collimator with a plane source positioned so that it is perpendicular to the collimator axis and adjacent to the base of the collimator.

The uncollided gamma-ray flux, as a function of position in the collimator, can be represented by an integral of the source angular distribution over the solid angle defined by the collimator, i.e.,

$$\Phi(R,z,\phi) = \int_{\Omega} \int S(\Omega) \sec \theta \, d^2\Omega \quad (\text{E-1})$$

where $S(\Omega)$ is the source angular distribution, $d^2\Omega$ is the differential solid angle and the angle θ is defined in Figure 13. Since only azimuthally independent source functions were considered then $S(\Omega) = S(\theta)$ and hence the flux was also azimuthally independent so $\Phi(R,z,\phi) = \Phi(R,z)$. It should be noted that Eq. (E-1) neglects both exponential attenuation and buildup due to air scattering.

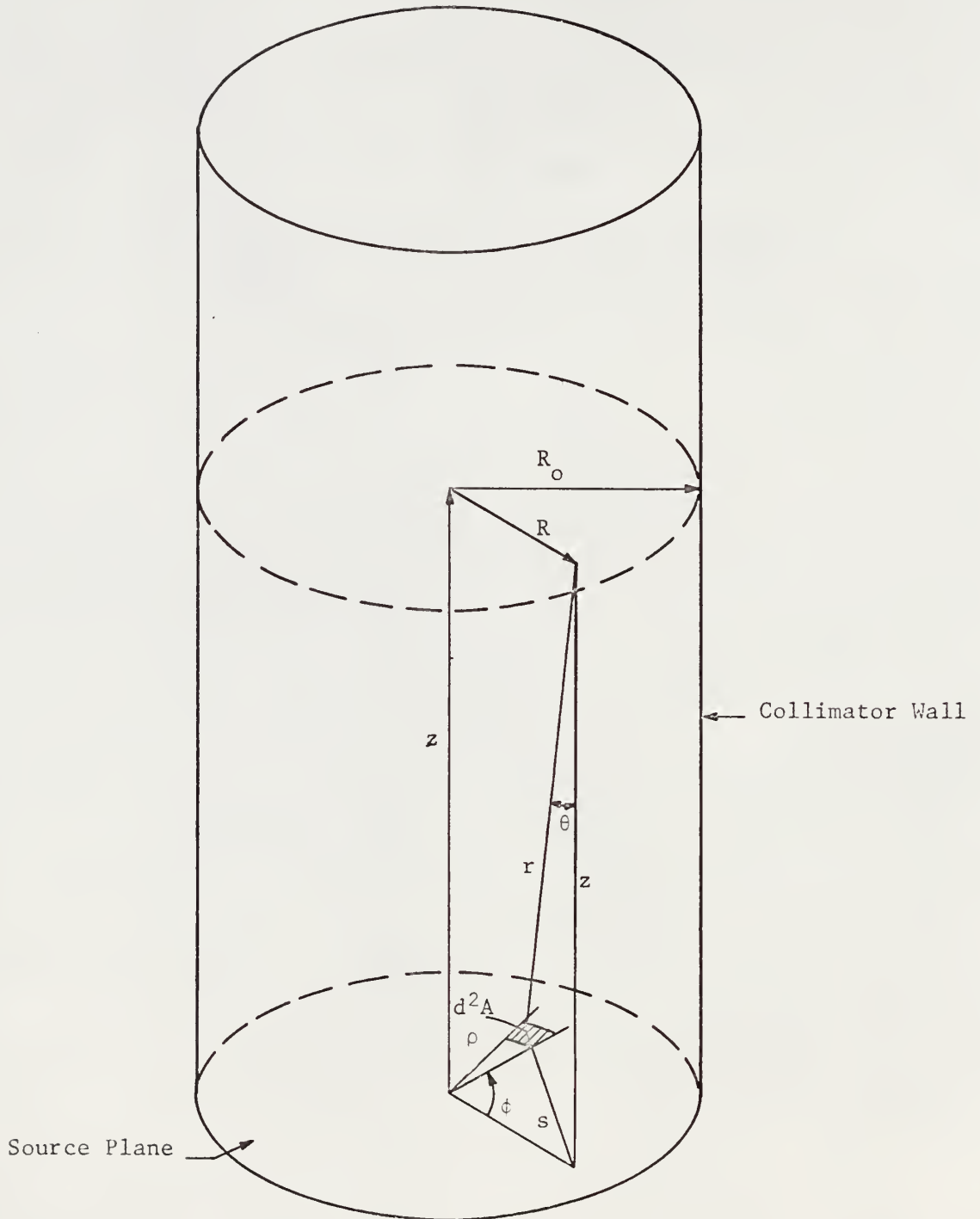


Figure 13. Collimator source geometry used in the derivation of the uncollided flux as a function of position P within the collimator

The differential solid angle can be written as

$$d^2\Omega = \frac{d^2A}{r^2} \cos \theta = \frac{\rho}{r^2} d\rho d\phi \cos \theta \quad (\text{E-2})$$

where d^2A , r , ρ , ϕ and θ are defined in Figure 13. Also from Figure 13 the following relation can be obtained

$$r^2 = z^2 + R^2 + \rho^2 - 2R\rho \cos \phi . \quad (\text{E-3})$$

Substitution of Eq. (E-2) into Eq. (E-1) and using Eq. (E-3) yields

$$\Phi(R, z) = \int_0^{R_0} \rho d\rho \int_0^{2\pi} \frac{S(\theta) d\phi}{[z^2 + R^2 + \rho^2 - 2R\rho \cos \phi]} . \quad (\text{E-4})$$

The three source functions considered were

$$S^{\text{I}}(\theta) = \frac{1}{4\pi} \quad (\text{E-5a})$$

$$S^{\text{II}}(\theta) = \frac{3}{4\pi} \cos^2 \theta \quad (\text{E-5b})$$

$$S^{\text{III}}(\theta) = \frac{5}{4\pi} \cos^4 \theta \quad (\text{E-5c})$$

where the angle θ is defined in Figure 13. These source functions are normalized such that integration of these functions over 4π steradians yields unity. Eq. (E-5a) represents an isotropic distribution whereas Eqs. (E-5b) and (E-5c) represent distributions which are peaked in the forward direction, i.e., the direction perpendicular to the source plane. From Figure 13 the following relation can be obtained,

$$\cos \theta = \frac{z}{r} = \frac{z}{[z^2 + R^2 + \rho^2 - 2R\rho \cos \phi]^{1/2}} . \quad (\text{E-6})$$

The fluxes resulting from the three source distributions given by Eqs. (E-5a), (E-5b) and (E-5c) are denoted by $\phi^{\text{I}}(R, z)$, $\phi^{\text{II}}(R, z)$ and $\phi^{\text{III}}(R, z)$ respectively. Substitution of these source distributions into Eq. (E-4) and using the relationship given by Eq. (E-6) yields

$$\phi^{\text{I}}(R, z) = \frac{1}{4\pi} \int_0^{R_0} \rho d\rho \int_0^{2\pi} \frac{d\phi}{[z^2 + R^2 + \rho^2 - 2R\rho \cos \phi]} \quad (\text{E-7a})$$

$$\phi^{\text{II}}(R, z) = \frac{3z^2}{4\pi} \int_0^{R_0} \rho d\rho \int_0^{2\pi} \frac{d\phi}{[z^2 + R^2 + \rho^2 - 2R\rho \cos \phi]^2} \quad (\text{E-7b})$$

$$\phi^{\text{III}}(R, z) = \frac{5z^4}{4\pi} \int_0^{R_0} \rho d\rho \int_0^{2\pi} \frac{d\phi}{[z^2 + R^2 + \rho^2 - 2R\rho \cos \phi]^3} \quad (\text{E-7c})$$

Eqs. (E-7a), (E-7b) and E-7c) were made dimensionless through the transformation of variables given by

$$v = \frac{R}{R_0}, \quad \xi = \frac{z}{R_0}, \quad \mu = \frac{\rho}{R_0} \quad (\text{E-8})$$

Application of this transformation of variables to the flux equations yields

$$\phi^{\text{I}}(v, \xi) = \frac{1}{4\pi} \int_0^1 \mu d\mu \int_0^{2\pi} \frac{d\phi}{[\xi^2 + v^2 + \mu^2 - 2v\mu \cos \phi]} \quad (\text{E-9a})$$

$$\phi^{\text{II}}(v, \xi) = \frac{3\xi^2}{4\pi} \int_0^1 \mu d\mu \int_0^{2\pi} \frac{d\phi}{[\xi^2 + v^2 + \mu^2 - 2v\mu \cos \phi]^2} \quad (\text{E-9b})$$

$$\phi^{\text{III}}(v, \eta) = \frac{5\xi^4}{4\pi} \int_0^1 \mu d\mu \int_0^{2\pi} \frac{d\phi}{[\xi^2 + v^2 + \mu^2 - 2v\mu \cos \phi]^3} \quad (\text{E-9c})$$

Carrying out the integrations in the expressions for the fluxes given above yields

$$\phi^I(v, \xi) = \frac{1}{4} \ln \left\{ \frac{\sqrt{(v^2-1)^2 + \xi^4 + 2\xi^2(1+v^2)} + \xi^2 - v^2 + 1}{2\xi^2} \right\} \quad (\text{E-10a})$$

$$\phi^{II}(v, \xi) = \frac{3}{8} \left\{ 1 - \frac{\xi^2 + v^2 - 1}{[(\xi^2+1)^2 + (v^2-1)^2 + 2\xi^2v^2 - 1]^{1/2}} \right\} \quad (\text{E-10b})$$

$$\begin{aligned} \phi^{III}(v, \xi) = \frac{5}{16} \left\{ \frac{(1+\xi^2-v^2) [(\xi^2+1)^2 + v^4 + 2v^2(2\xi^2-1)] - 2\xi^4(\xi^2+1+3v^2)}{[(\xi^2+1)^2 + v^4 + 2v^2(\xi^2-1)]^{1/2}} \right. \\ \left. - \frac{(\xi^2-v^2)(\xi^4+4\xi^2v^2+v^4) - 2\xi^4(\xi^2+3v^2)}{(\xi^2+v^2)^3} \right\} \quad (\text{E-10c}) \end{aligned}$$

From these three expressions the uncollided gamma-ray flux can be determined for any point in the collimator in terms of the dimensionless parameters v and ξ which are directly proportional to the radial and axial position of the point in the collimator.

Now consider the collimator-plane source geometry used in the dosimeter calibration of Section 5.0 and that used for the scattered gamma-ray measurements of Section 6.0. In these two cases the source plane was not located adjacent to the base of the collimator, however, as Eq. (E-1) was based on an integration over the solid angle the distance from the source to the point of interest is not a factor in determining the flux as long as the solid angle remains constant.

In the dosimeter calibration of Section 5.0 a plane isotropic source was used. On the other hand, theoretical studies (17,18) indicate that the angular distribution for radiation scattered from a concrete slab is not isotropic. In fact for the experimental configurations considered in this

work it appears that the angular distribution of the scattered radiation is proportional to $\sec^n \theta$ where θ is the angle that the scattered radiation makes with the perpendicular to the scattering plane. Now recall that for the scattered radiation measurements the scattering surface was not perpendicular to the collimator axis but rather it was at an angle of 72° to the collimator axis in each of the experimental configurations considered. Then based on this fact and the previously mentioned theoretical studies found in the literature, the effective source seen by a detector located in the collimator should have an angular distribution which is peaked in the direction of the detector. Although the analytic form of this angular distribution is not known, the theoretical studies (17,18) indicate that it is not as highly peaked in the direction of the detector as the $\cos^4 \theta$ distribution considered in the derivation of Eq. (E-10c). Hence it appears that Eq. (E-10a) is applicable to the calibration experiment and that Eq. (10-c) should provide an approximate upper limit with respect to the peaking of the angular distributions encountered in the scattered gamma-ray measurements.

Now since the purpose of this appendix was to determine if the spatial distribution of the uncollided gamma-ray flux varied as the angular distribution of the plane source was changed, Eqs. (E-10a), (E-10b) and (E-10c) were evaluated for different positions in the collimator. In order that the results of these computations could be used in support of the experimental techniques used in this work, the flux was determined for various points in a particular right circular cylindrical volume of the collimator. This volume corresponds to the volume occupied by the dosimeter during the experimental measurements of Sections 5.0 and 6.0. (See Figure 6.) Calculations

were made for points along the centerline ($\nu=0$), edge ($\nu=1$) and base of this cylindrical volume. So that the results from the different plane source angular distributions could be readily compared, the fluxes at the various points considered were normalized to the flux at the center of the volume ϕ_c for each of the source distributions. Table E-I is a tabulation of these normalized fluxes for the three plane source angular distributions considered.

Table E-I. Normalized fluxes as a function of position in the collimator and plane source angular distribution.

$$\phi_c^I = 0.86356 \times 10^{-3} \text{ gammas/cm}^2\text{-sec}$$

$$\phi_c^{II} = 2.5862 \times 10^{-3} \text{ gammas/cm}^2\text{-sec}$$

$$\phi_c^{III} = 4.3029 \times 10^{-3} \text{ gammas/cm}^2\text{-sec}$$

ξ	$\frac{\phi^I(\nu=0, \xi)}{\phi_c^I}$	$\frac{\phi^{II}(\nu=0, \xi)}{\phi_c^{II}}$	$\frac{\phi^{III}(\nu=0, \xi)}{\phi_c^{III}}$
15.625	1.1834	1.1830	1.1826
16.175	1.1044	1.1042	1.1040
16.725	1.0331	1.0330	1.0330
17.275	.96847	.96852	.96857
17.825	.90972	.90986	.91001
18.375	.85615	.85636	.85658
ξ	$\frac{\phi^I(\nu=1, \xi)}{\phi_c^I}$	$\frac{\phi^{II}(\nu=1, \xi)}{\phi_c^{II}}$	$\frac{\phi^{III}(\nu=1, \xi)}{\phi_c^{III}}$
15.625	1.1786	1.1734	1.1684
16.175	1.1002	1.0959	1.0916
16.725	1.0294	1.0257	1.0221
17.275	.96525	.96211	.95898
17.825	.90688	.90419	.90153
18.375	.85364	.85134	.84907

Table E-1 (continued)

ν	$\frac{\phi^{\text{I}}(\nu, \xi=15.625)}{\phi_c^{\text{I}}}$	$\frac{\phi^{\text{II}}(\nu, \xi=15.625)}{\phi_c^{\text{II}}}$	$\frac{\phi^{\text{III}}(\nu, \xi=15.625)}{\phi_c^{\text{III}}}$
0.0	1.1834	1.1830	1.1826
0.2	1.1832	1.1826	1.1820
0.4	1.1826	1.1815	1.1803
0.6	1.1816	1.1795	1.1775
0.8	1.1803	1.1769	1.1735
1.0	1.1786	1.1734	1.1684

From a comparison of the values of ϕ_c^{I} , ϕ_c^{II} , and ϕ_c^{III} given in Table E-1, it can be seen that the flux increases as the angular distribution of the plane source becomes more highly peaked in the direction perpendicular to the source plane. However, the values of the normalized fluxes $\phi^{\text{I}}(\nu, \xi)/\phi_c^{\text{I}}$, $\phi^{\text{II}}(\nu, \xi)/\phi_c^{\text{II}}$ and $\phi^{\text{III}}(\nu, \xi)/\phi_c^{\text{III}}$ for any point in that portion of the collimator volume under consideration were in close agreement to one another. In fact a comparison of these three ratios for any of the points (ν, ξ) considered in Table E-1 always resulted in an agreement between them which was less than one per cent. Therefore it can be concluded that for the collimator-plane source systems considered in this appendix a change in the angular distribution of the plane source results in a negligible change in the spatial distribution of the flux within the collimator volume considered.

Now it has been pointed out that the plane isotropic source case was applicable to the dosimeter calibration of Section 5.0 and that the distribution should provide an upper limit with reference to the peaked angular distributions of the effective plane sources in the scattered radiation measurements of Section 6.0. Also the numerical results presented in Table E-1 indicated that the spatial distribution of the flux throughout the

volume which the dosimeter would occupy is the same for the three angular distributions considered. Thus the conclusions resulting from this study can be extended to the work done in the remainder of this report by stating that in both the dosimeter calibration of Section 5.0 and the scattered radiation measurements of Section 6.0 the spatial distribution of the uncollided gamma-ray flux throughout the volume of the dosimeter was essentially the same. Hence it can be concluded that the application of the calibration curves developed in Section 5.0 and used to analyze the dosimeter responses obtained from the scattered radiation measurements of Section 6.0 was valid even though the angular distributions of the plane sources considered in Sections 5.0 and 6.0 were not the same.

EVALUATION OF EXPOSURE DOSES RESULTING FROM SCINTILLATION AND
IONIZATION DETECTOR MEASUREMENTS OF COMPLEX GAMMA-RAY SPECTRA

by

WILLIAM THOMAS URBAN

B. S., Kansas State University, 1964

AN ABSTRACT OF
A MASTER'S THESIS

submitted in partial fulfillment of the
requirements for the degree

MASTER OF SCIENCE

Department of Nuclear Engineering

KANSAS STATE UNIVERSITY

Manhattan, Kansas

1969

ABSTRACT

A study was made to determine experimentally the validity of using an unfolding technique, developed for the analysis of data obtained using a collimator-spectrometer system, in the computation of exposure doses. This determination was based on a comparison between exposure doses computed from experimental complex gamma-ray energy spectra using the unfolding technique and exposure doses resulting from measurements with an air equivalent ionization chamber (dosimeter).

The experimental phase of this work consisted of measuring exposure doses for various gamma-ray energy distributions using both an NaI(Tl) scintillation detector and a dosimeter. An energy distribution of gamma rays was obtained by scattering cobalt-60 radiation from a concrete slab. The two detection instruments were placed (alternately) in a lead collimator to enable the measurement of gamma-ray energy distributions corresponding to three different experimental configurations.

An expression was derived relating the response of the dosimeter to a plane monoenergetic source to its response to a plane polyenergetic source of equivalent strength and known energy distribution. Using this expression calibration equations relating dosimeter response to exposure dose were obtained for each of the energy distributions to be considered by exposing the dosimeter to a simulated plane isotropic source of cobalt-60. The validity of this calibration technique for the dosimeter was examined in detail.

As a result of the comparison between the exposure doses obtained using the dosimeter and those obtained by applying the unfolding technique to the

complex spectra measured it was found that the unfolding technique under consideration resulted in exposure doses which were substantial overestimations of those obtained using the dosimeter. This overestimation appeared to be systematic and it was concluded that the most probable source of this error was in the normalization of the response functions and/or in the generation of the response matrix.

